DOI: 10.1002/ejoc.201000233

Self-Assembling Depsipeptide Dendrimers and Dendritic Fullerenes with New *cis*- and *trans*-Symmetric Hamilton Receptor Functionalized Zn–Porphyrins: Synthesis, Photophysical Properties and Cooperativity Phenomena

Katja Maurer,[a] Bruno Grimm,[b] Florian Wessendorf,[a] Kristine Hartnagel,[a] Dirk M. Guldi,*[b] and Andreas Hirsch*[a]

Keywords: Dendrimers / Fullerenes / Porphyrinoids / Hydrogen bonds / Self-assembly / Cooperative effects

Two novel supramolecular building blocks, namely *cis*- and *trans*-symmetric zinc–porphyrins bearing Hamilton receptors as their focal points (**10** and **15**), were self-assembled with (i) first-, second- and third-generation depsipeptide cyanurates (**21**–**23**); (ii) second-generation dendrofullerene (**24**), and (iii) cyanuric acid substituted fullerene (**20**), and probed in a series of photophysical investigations. Importantly, an overall 1:2 stoichiometry was confirmed with binding constants K_n, and Hill coefficients n_H that indicate remarkable cooperativities. As a general feature, stronger binding evolves from the *trans*-symmetric porphyrin isomer, although the increased steric demand of the depsipeptide ligands means that the binding constants decrease with each generation. The self-assembly of **10** or **15** with **20** affords novel electron donor–acceptor hybrids that reveal, upon excitation, intra-hybrid charge-transfer events.

Introduction

Combining the rapidly evolving fields of nanostructured materials and supramolecular chemistry is an attractive strategy for constructing large and complex, yet highly ordered, molecular and supramolecular entities with defined functions. Specifically, developing novel super- and supramolecular electron donor–acceptor architectures – based on functional dyes – through careful design have emerged as viable tools for efficient conversion of solar energy.[1] In this context, porphyrins, owing to their biological relevancy[2] and remarkable photoelectronic properties,[3] have stimulated great interest in devising, designing, synthesizing and testing porphyrin-containing supramolecular electron donor–acceptor architectures. To this end, several facts of multifunctional porphyrin assemblies – built on hydrogen-bonding – have been explored with great success.[4] Likewise, covalent motifs have been employed for the preparation of porphyrin–dendrimer conjugates that function as synthetic mimics of globular heme proteins.[5] Dendrimer-like structures, i.e, zinc–porphyrin cores bearing different Fréchet-type dendrons, were also studied with respect to unidirectional transfer of excited-state energy.[6] Here, a superb example is a dendritic architecture, where the use of up to eight boron-dipyrrin chromophores has been used to mimic the basic functions of the natural photosynthetic antenna complexes.[7]

Porphyrins endowed with Hamilton receptors have been integrated into enzymatic models[8] and/or into photoactive systems.[9] Our own contribution to this highly interdisciplinary field started with first, second, and third generations of depsipeptide dendrons and their self-assembly with a homotritopic Hamilton receptor.[10a] Here, chiroptical investigations stood at the forefront. Conditions that enforce the aggregation of these depsipeptide cyanurates with, for example, the Hamilton receptor carrying porphyrin led to the formation of different chiral porphyrin dendrimers.[10b]

The photophysical and (opto)electronic properties of metalloporphyrins are truly unique, especially when they are combined with fullerenes.[11] What renders fullerenes exceptional is their capability to reversibly accept up to six electrons,[12] while exhibiting a low reorganization energy that is associated with each of these electron-transfer steps.[13] As a matter of fact, a considerable number of electron donor–acceptor conjugates – based on combinations of porphyrins and fullerenes – emerged in recent years that combine all the key functions of the photosynthetic reaction center, that is, light-harvesting and charge-transfer.[14] Hydrogen bonding is, however, hardly ever employed to integrate the different building blocks (i.e., porphyrins and fullerenes) into fully operational reaction center models.[15] One of the few examples is a chiral fullerene dendron.[16]

[a] Department of Chemistry and Pharmacy, and Interdisciplinary Center of Molecular Materials (ICMM), Friedrich-Alexander-Universität Erlangen-Nürnberg,
Henkestrasse 42, 91054 Erlangen, Germany
E-mail: dirk.guldi@chemie.uni-erlangen.de
andreas.hirsch@chemie.uni-erlangen.de
[b] Department of Chemistry and Interdisciplinary Center of Molecular Materials (ICMM), Friedrich-Alexander-Universität Erlangen-Nürnberg,
Egerlandstrasse 3, 91058 Erlangen, Germany
Supporting information for this article is available on the WWW under http://dx.doi.org/10.1002/ejoc.201000233.

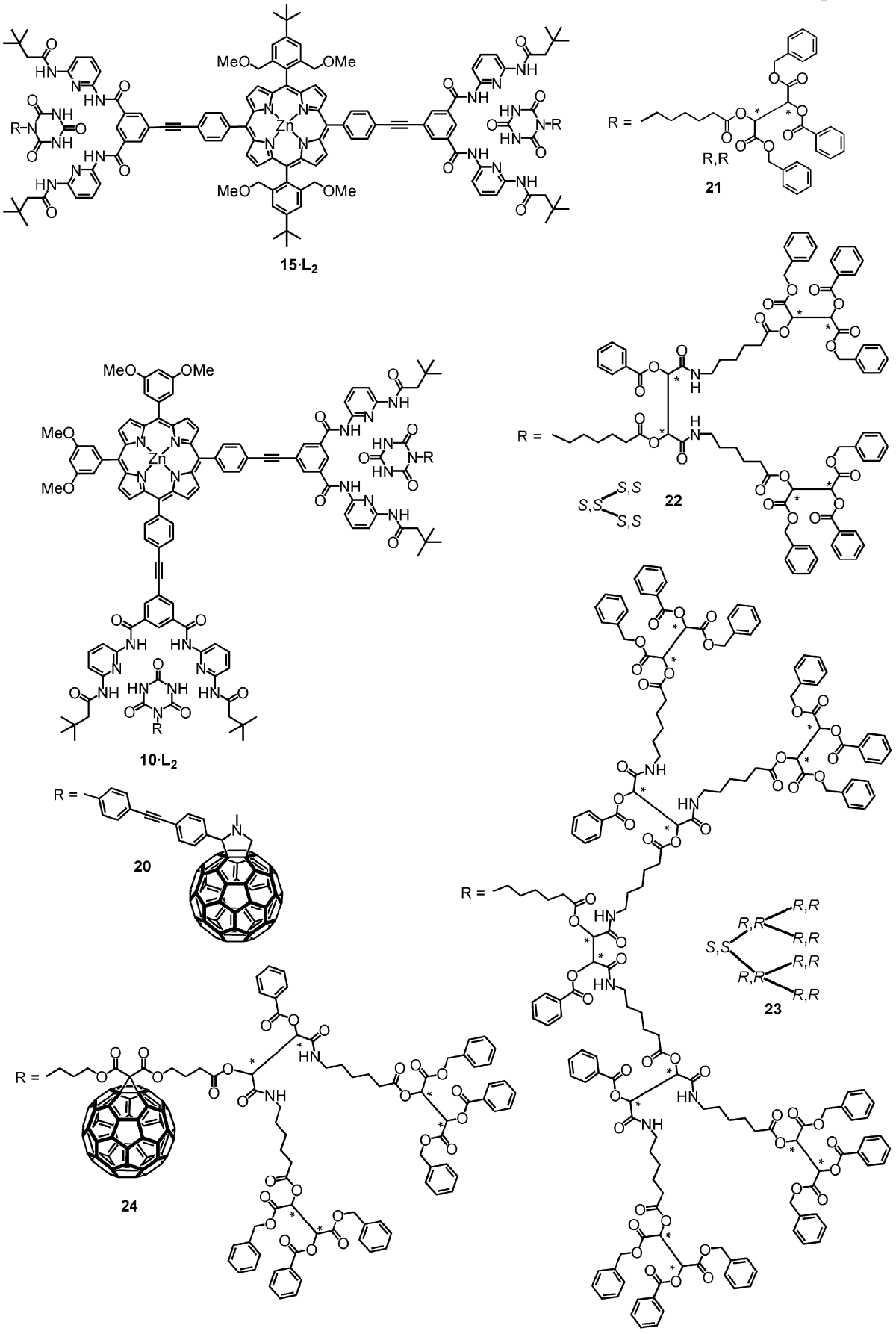

Figure 1. Supramolecular complexes of the Hamilton receptor functionalized Zn–porphyrins **10·L$_2$** and **15·L$_2$**.

Placing cyanuric acid functionalities at the focal points of these dendrons guarantees control of the directed self-assembly of Hamilton receptor functionalized metalloporphyrins [i.e., tin porphyrin (SnP) and zinc porphyrin (ZnP)].[17] In this context, we reported the modular self-assembly of depsipeptide dendrons on a Hamilton receptor modified porphyrin platform – realized with an SnP functionalized with two axial Hamilton receptors.[17b] With the help of a detailed time-resolved fluorescence and transient absorption investigation we documented that, in the corresponding SnP/fullerene hybrids, energy transfer rather than electron transfer dominates the excited-state features.

In the current work, we wish to introduce two novel supramolecular ZnP building blocks **10** and **15**, namely *cis*- and *trans*-zinc–porphyrin isomers bearing two Hamilton receptor functionalities as their focal points as a complement to the previously published Hamilton receptor functionalized porphyrins.[17] The *cis* versus *trans* symmetry of **10** and **15** represents a substitution pattern that deserves particular attention with respect to the generation of novel supramolecular architectures. When, for example, a *cis*-symmetric Hamilton receptor and a complementary bis(cyanuric acid) building block are used, it is likely that rectangular architectures should evolve. This would, however, depend on the conformational flexibility/rigidity of the supramolecular aggregates. Photophysical events such as electron- and energy-transfer reactions have been shown to depend considerably on the character and flexibility of the linkage between the electron/energy donor and the electron/energy acceptor. Notably, high flexibility of the supramolecular hybrid might result in substantial inter/intramolecular folding. Further consequences, such as shorter lifetimes of the intermediately formed radical ion pair states or loss of control over supramolecular architectures, might be expected.[18] In light of the aforementioned considerations, rigid acetylene spacers were chosen for the covalent synthesis of the molecular building blocks **10**, **15**, and **20** (Figure 1). These are likely to restrict the flexibility of the Hamilton receptor and cyanuric acid functionalities and, at the same time, provide enhanced levels of electronic communication. The self-assembly processes of **10** and **15** with the depsipeptide dendrons (**21**–**23**) and second-generation dendrofullerene (**24**) and cyanuric acid substituted fullerene (**20**) were studied and, based on a detailed photophysical investigation, we conclude intrahybrid charge-transfer.

Results and Discussion

Synthesis of the Hamilton Receptor Substituted Porphyrin Derivatives

Scheme 1 sketches the synthetic route to the iodine-substituted Hamilton receptor derivative **3**,[19] which was used as a starting material for the targeted porphyrin guest molecules. In particular, heating of 5-iodobenzene-1,3-dioic acid (**1**)[20] with thionyl chloride ($SOCl_2$) at reflux, followed by coupling of the dichloride with *N*-(6-aminopyridin-2-yl)-3,3-dimethylbutanamide (**2**)[21] in tetrahydrofuran (THF) in situ afforded the iodine-substituted Hamilton receptor **3** in 73% isolated yield.

The synthesis of the *cis*-configured Hamilton receptor porphyrin is summarized in Scheme 2. 3,5-Dimethoxybenzaldehyde (**4**), 4-[2-(trimethylsilyl)ethynyl]benzaldehyde (**5**) and pyrrole (**6**) were treated with trifluoroacetic acid (TFA) in dichloromethane (CH_2Cl_2) under Lindsey conditions.[22] After 1 h, TFA was neutralized with an excess of triethylamine (NEt_3), and the reaction mixture was subjected to oxidation with 2,3-dichloro-5,6-dicyano-*p*-benzoquinone (DDQ). The porphyrin *cis* isomer was purified by repeated column chromatography on silica (SiO_2) using a mixture of hexane/ethyl acetate (8:2) as eluent. Metal insertion with zinc acetate [$Zn(OAc)_2$] followed by desilylation under inert conditions using a 1 M solution of tetrabutylammonium fluoride (TBAF) in THF led to the formation of porphyrin derivative **9** in good yield. Finally, **10** was obtained by a Sonogashira coupling reaction of **9** with the Hamilton receptor derivative **3** using tris(dibenzylidenacetone)dipalladium(0) [$Pd_2(dba)_3$] and triphenylarsane ($AsPh_3$) as catalysts. The target compound **10** was isolated by repeated column chromatography on SiO_2 in 38% yield. TLC monitoring of the Sonogashira reaction was impossible; therefore, the progress of the reaction was monitored by FAB MS. After 24 h, the FAB mass spectra of the crude reaction mixture revealed a peak corresponding to the $[M]^+$ ion of target molecule **10** with, however, low intensity. During the progress of the reaction, the intensity of the $[M]^+$ peak corresponding to **10** barely changed. Therefore, longer reaction times were required to guarantee completion of the coupling reaction.

The synthetic route to the *trans*-configured Hamilton receptor substituted porphyrin **15** barely differs from that of

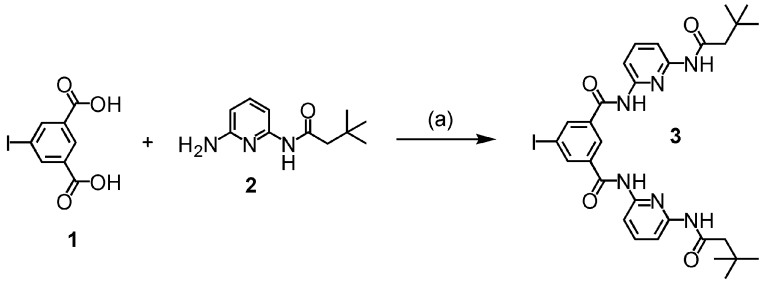

Scheme 1. Synthesis of the iodine-substituted Hamilton receptor derivative **3**. Reagents and conditions: (a) $SOCl_2$, DMF, NEt_3, THF, room temp., 72 h, 73%.

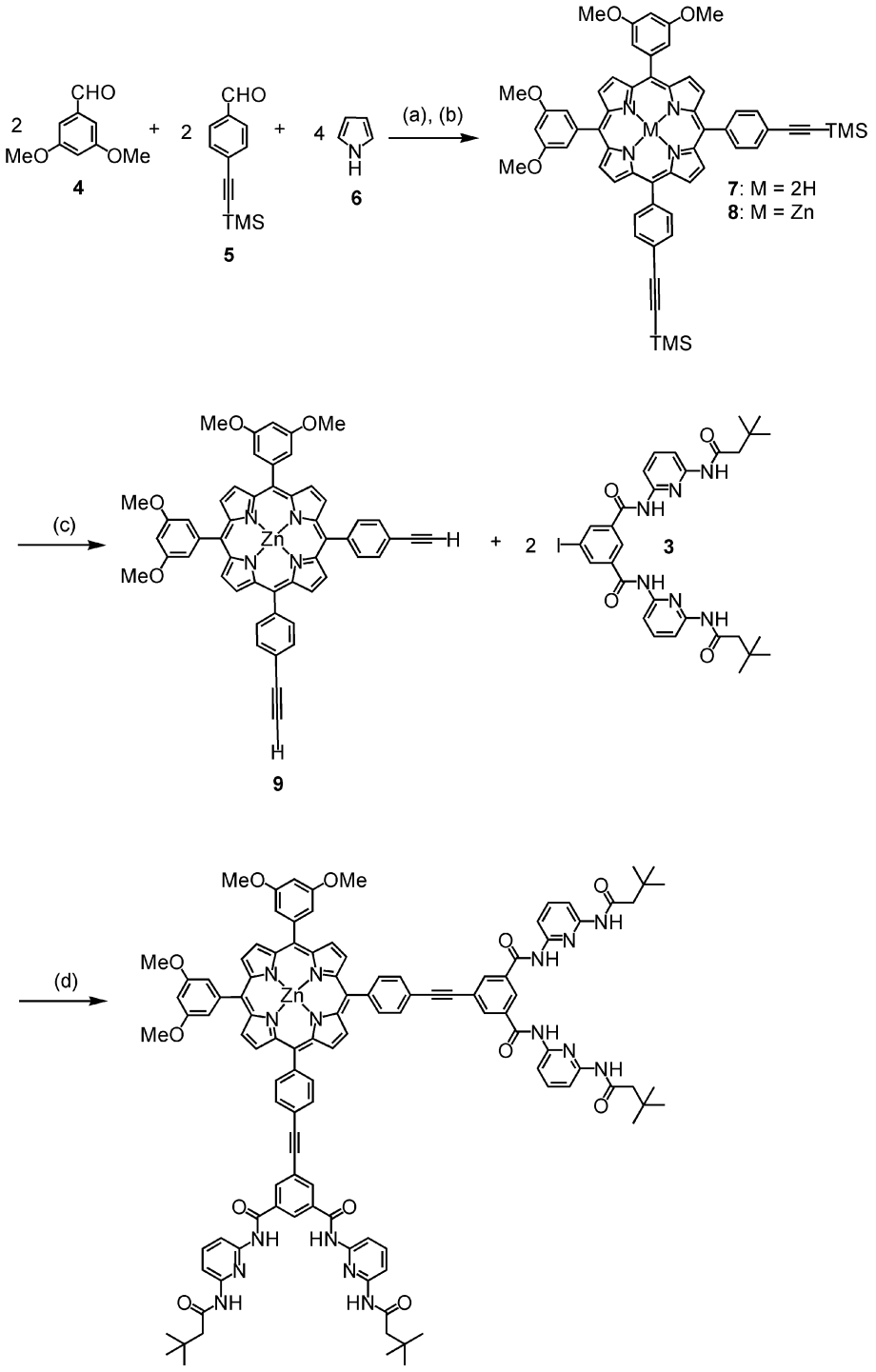

Scheme 2. Synthesis of Hamilton receptor substituted porphyrin **10**. Reagents and conditions: (a) TFA, CH_2Cl_2, 1 h; NEt_3, DDQ, room temp., 2 h, 9%; (b) $Zn(OAc)_2$, THF, reflux, 1.5 h, 93%; (c) TBAF (1 M, THF), THF, r.t., 12 h, 93%; (d) $Pd_2(dba)_3$, $AsPh_3$, THF/NEt_3 (2:1), 6 d, 38%.

10 (Scheme 3). Dipyrromethane **11**[23] was chosen for two reasons: (i) The *tert*-butyl groups should guarantee good solubility and low polarity of the porphyrin intermediates. (ii) Literature reports[23] have documented the stability of **11** during scrambling processes, which leads to the conclusion that the formation of statistical side products is inhibited and that the formation of the desired *trans* isomer **12** is favored. Again, the Sonogashira coupling reaction of **3** and **14** was monitored by FAB MS, and the target compound **15** was isolated in 31% yield by repeated column chromatography on SiO_2. The Hamilton receptor substituted zinc–porphyrins **10** and **15** were characterized spectroscopically (i.e., ^1H and ^{13}C NMR, UV/Vis and IR spectroscopy), complemented by elemental ananlysis, FAB and

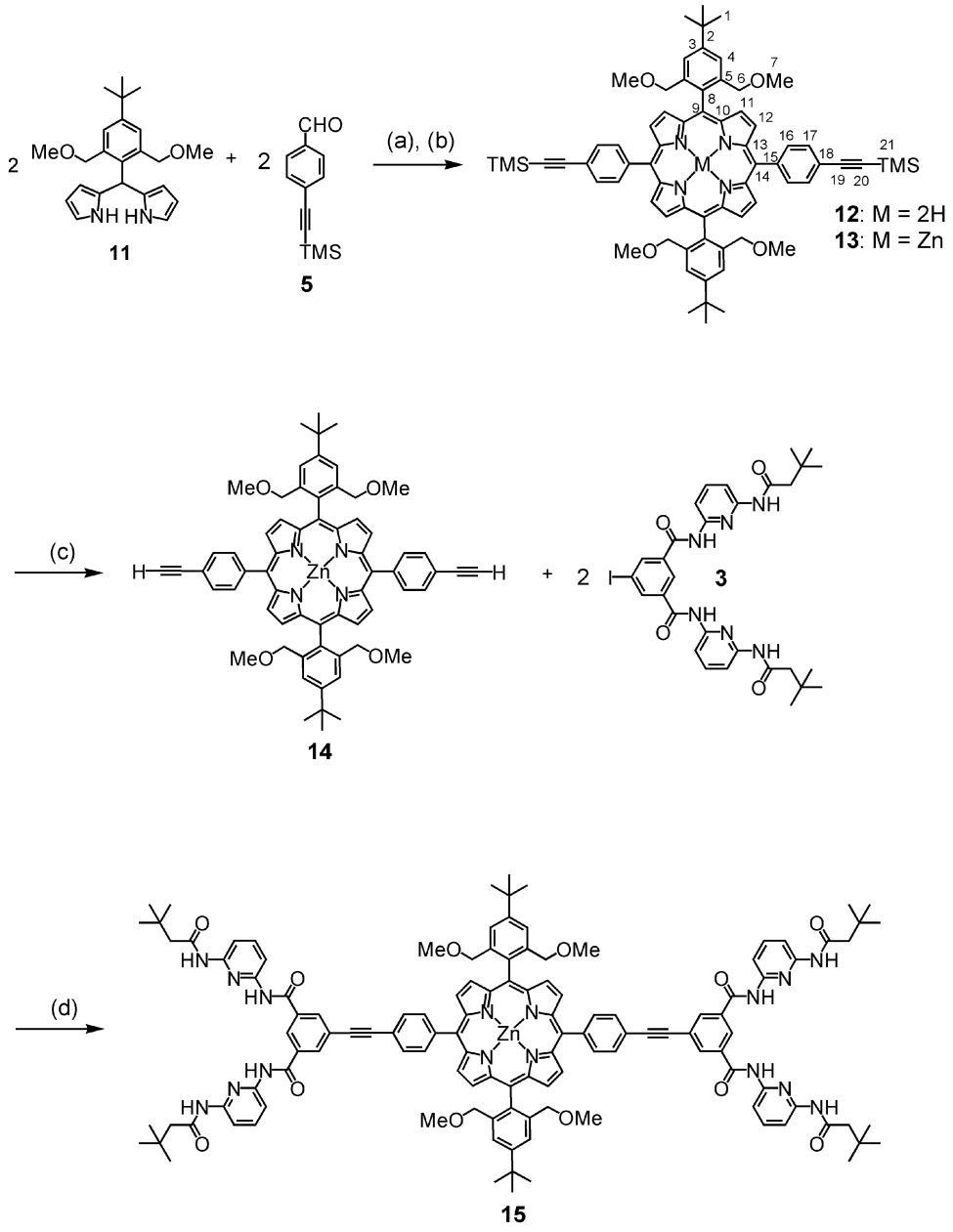

Scheme 3. Synthesis of the Hamilton receptor substituted porphyrin **15**. Reagents and conditions: (a) TFA, CH_2Cl_2, 1 h, room temp.; NEt_3, DDQ, 2 h, r.t., 10%; (b) $Zn(OAc)_2$, THF, reflux 12 h, 83%; (c) TBAF (1 M, THF), THF, 12 h, r.t., 79%; (d) **3**, $Pd_2(dba)_3$, $AsPh_3$, THF/NEt_3 (2:1), 6 d, r.t., 31%.

MALDI TOF mass spectrometry. All ^1H and ^{13}C NMR assignments were guided by HETCOR and COSY analyses.

The characterization of **13**, **14**, and **15** (i.e., ZnP) by ^1H NMR spectroscopy in deuterated chloroform ($CDCl_3$) led to unresolved and broad resonance signals. However, the ^1H NMR spectra of **12** (i.e., H_2P) showed the expected resolution and splitting pattern. The low solubility of **13**, as a possible rationale, is ruled out on the basis that the corresponding solutions prior to and after the measurements were clear with no appreciable signs of aggregate formation, etc. Less concentrated $CDCl_3$ solutions of **13** led to the same features. The same phenomenon was also observed in the ^{13}C NMR spectra.

Compound **13** was also investigated by using temperature-dependent ^1H NMR measurements in the range between –40 and +50 °C in $CDCl_3$ (Figure 2). At very low temperatures, all resonances were broad and unresolved. Importantly, over the entire temperature range the TMS resonance signal at δ = 0.4 ppm remained unaffected. Upon increasing the temperature above +50 °C the signals of the aromatic protons (i.e., δ = 7.8–8.7 ppm) sharpened, while the signal of the pyrrol protons (i.e., 11 at δ = 8.5 ppm) remained unresolved. At 30 °C, the resonances of the phenyl protons 4 at δ = 7.5 ppm become visible in the form of broad, unresolved signals, which shift slightly to lower fields with further increasing temperature. Concerning the

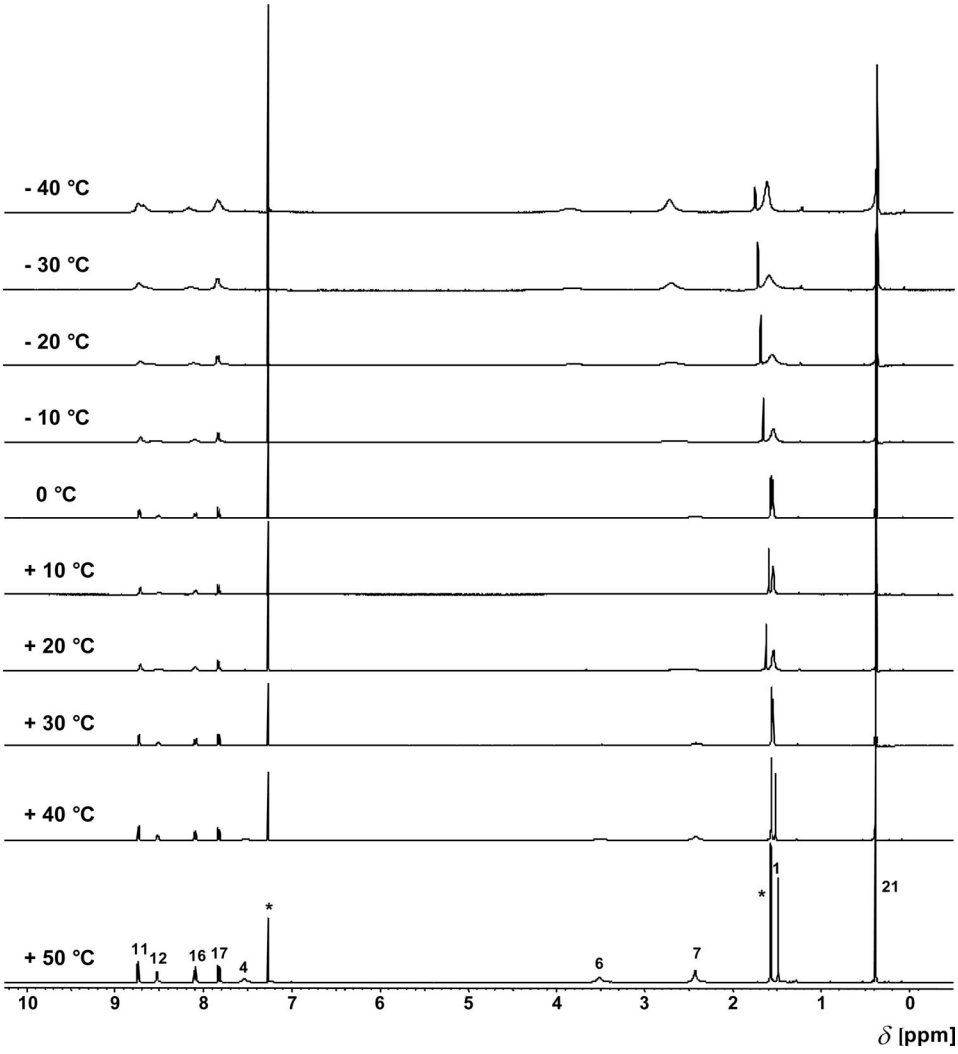

Figure 2. Temperature-dependent ^{1}H NMR spectra (400 MHz, $CDCl_3$) of **13**.

alkyl protons 1, 6, 7 and 21, no clear tendency was, however, discerned. For example, the resonance signals of the alkyl protons 6 and methyl protons 7 are barely visible at δ = 3.5 and 2.4 ppm, respectively, between –40 and –20 °C. At higher temperatures, a notable broadening and slight shifts to higher fields were observable. In the range of –10 °C to +20 °C it was impossible to differentiate between the signal and the baseline. At +30 °C the resonances were visible again but remained unresolved even at +50 °C. In the low-temperature regime, the resonances of the *tert*-butyl protons 1 could be observed as a broad signal at δ = 1.4 ppm. When the temperature was increased to +50 °C, the resonances became sharp and were slightly shifted to lower fields.

Because the free-base porphyrin **12** did not exhibit the same temperature-dependent NMR spectral changes, we considered the coordination chemistry of zinc as a possible rationalization. Zinc–porphyrins are known to coordinate neutral ligands, such as N, O, S, P donors, and charged ligands through axial coordination. However, the binding strengths in nonpolar solvents such as chloroform ($CHCl_3$) and CH_2Cl_2 were found to increase in the order S, P < O < N[24]and, therefore, the addition of amines such as pyridine should lead to ligand-exchange reactions. Only a few examples of six-coordinate Zn–porphyrin complexes are described in the literature.[25] Nickel, on the other hand, favors the formation of square-planar complexes.[11] This prompted us to synthesize **16** and characterize it by means of NMR spectroscopy (Figure 3). As expected, sharp and well-resolved peaks evolve in the ^{1}H and ^{13}C NMR spectra of **16**.

According to PM3 calculations[26] on the geometry-optimized structure of **13**, intramolecular donor–acceptor bonding involving the methoxy oxygen atom and the axial coordination site of the zinc ion is restricted. It is notable that the free rotation of the *tert*-butyl-substituted phenyl rings is hindered. Steric repulsion between the α-pyrrol proton and the methoxy substituents is likely to be responsible for this phenomenon.[23] Hence, we excluded the presence of different rotational isomers in solution. Further semiempirical PM3 calculations[27] performed on a Zn–porphyrin dimer of **13**/**13**, resulted in a calculated 2.0 Å distance be-

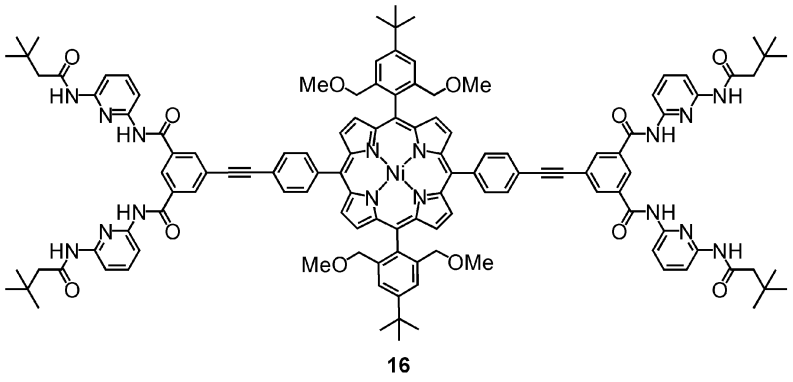

Figure 3. Ni–porphyrin **16**.

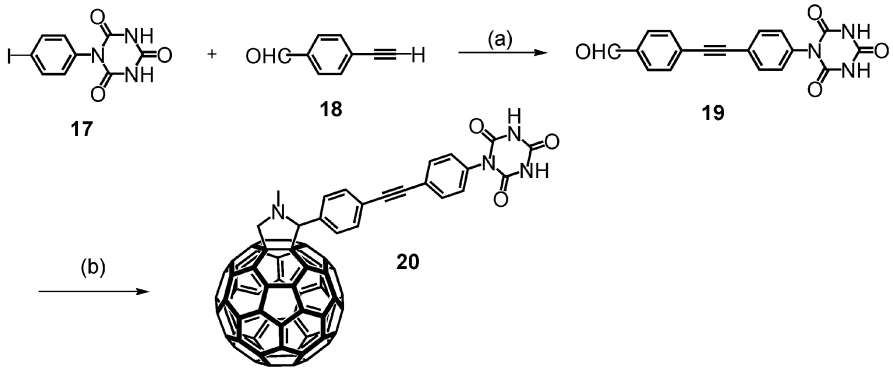

Scheme 4. Synthesis of the cyanuric acid substituted fullerene **20**. Reagents and conditions: (a) $Pd(PPh_3)_2Cl_2$, CuI, THF/NEt_3, room temp., 73%; (b) fullerene, sarcosine, toluene/THF, reflux 29%.

tween the zinc ion and the coordinated methoxy oxygen atom. Therefore, particularly strong intermolecular interactions are considered likely.

Scheme 4 depicts the synthesis of cyanuric acid substituted fullerene **20**. Sonogashira coupling of the 4-iodophenyl isocyanuric acid **17**[28] with aldehyde **18** in the presence of bis(triphenylphosphane)palladium(II) dichloride [$Pd(PPh_3)_2Cl_2$] as a catalyst led to the formation of the cyanuric acid substituted aldehyde **19** in good yields. The azomethine ylide of **18**, which was formed in situ, and sarcosine were treated with fullerene to afford the target compound **20**, which was purified by column chromatography on SiO_2.

Determination of Association Constants and Cooperativity of Binding

The association constants and the cooperativity of the supramolecular **10·L₂** and **15·L₂** complexes (**L** = **21**, **22**, and **23**)[10a] were determined by ^{1}H NMR titration experiments[29] in $CDCl_3$. The experiments were performed by the stepwise addition of 40 μL of a 2.5 mM solution of **21**–**23** to 0.5 mL of a 0.5 mM solution of **10** or **15** in $CDCl_3$. Hamilton receptors tend to form rather stable intermolecular aggregates through multiple hydrogen bonds in apolar, noncoordinating solvents such as $CDCl_3$.[10a,17b,19] As a consequence, rather broad and unresolved ^{1}H NMR peaks emerge (see Figures 4 and 5). Complexation of the corresponding cyanurate guest, on the other hand, promotes dissociation of the intermolecular aggregates and is accompanied by a noticeable sharpening of the resonance signals. The NH^1 and the NH^2 resonances of the Hamilton receptor undergo a continuous downfield shift until the 1:2 complexes prevail. After the addition of 0.4 equiv. of **21**, the signal of the NH^3 protons of the cyanuric moiety is observed at δ = 13.4 ppm. In contrast to the amide protons of the Hamilton receptor, the resonance of the NH^3 protons experiences a high-field shift and increased broadening due to fast exchange processes between free and bound cyanurate. Nevertheless, the average signal disappears after the addition of 2.4 equiv. of the guest molecule. The supramolecular hydrogen-bonded assemblies undergo continuous self-assembly and disassembly processes[30] and the dynamic character of these systems is revealed by temperature-dependent ^{1}H NMR spectroscopy. Figure 5 shows the coordination motif and the ^{1}H NMR spectra of a 1:8 mixture of **10** and **21** at various temperatures. Below 0 °C, the NH^1 and NH^2 protons of the Hamilton receptor are observed as broad and unresolved signals. Upon increasing the temperature to 20 °C these resonances sharpen. In the temperature range between –40 and 20 °C the two resonance signals relate to the free and bound NH^3 protons of the cyanuric moiety. Here, a slow (on the NMR time-scale) association/disassociation equilibrium is inferred. Above 0 °C, the NH^3

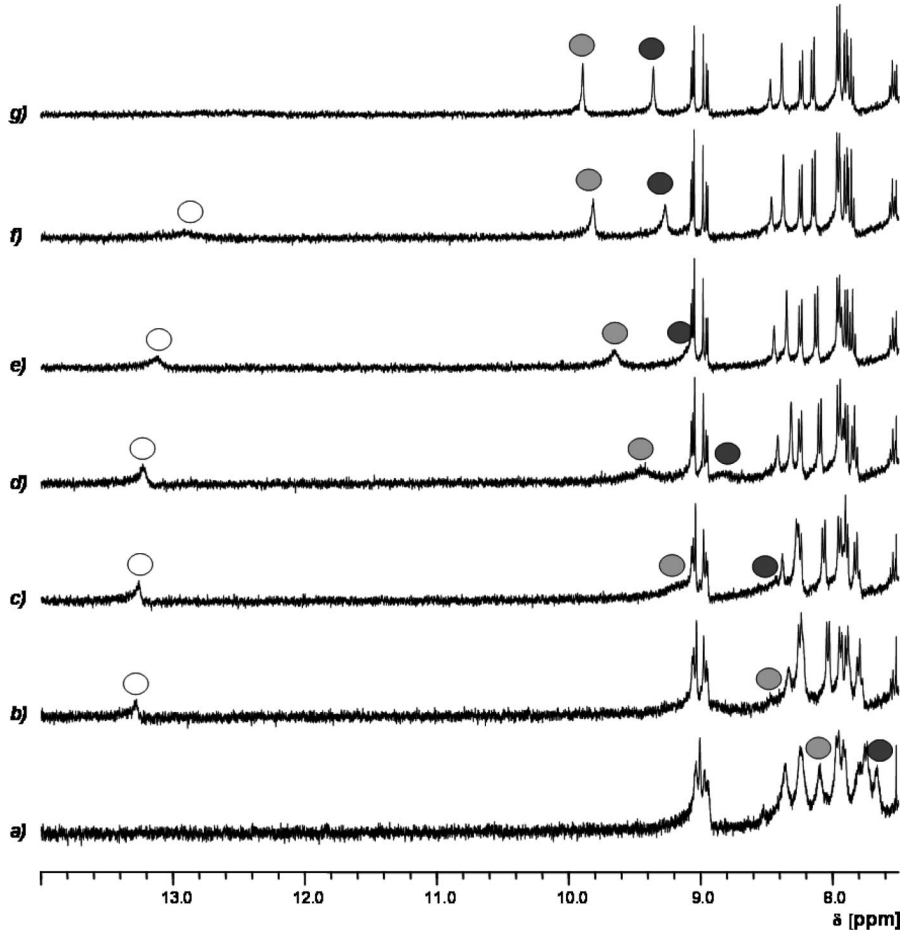

Figure 4. Chemical shifts of the NH^1, NH^2, and NH^3 signals during the titration of **10** with the guest molecule **21** (^{1}H NMR spectra, 400 MHz, $CDCl_3$). After the addition of **21**: (a) 0 equiv.; (b) 0.4 equiv.; (c) 0.8 equiv.; (d) 1.2 equiv.; (e) 1.6 equiv.; (f) 2.0 equiv.; (g) 2.4 equiv.

resonances of the cyanuric moiety become very broad and can no longer be detected. Temperature-dependent ^{1}H NMR spectroscopy analyzing similar supramolecular complexes in the range of –60 to 90 °C using deuterated dichloroethane as a solvent verified that the temperature interval of 0–50 °C represents a coalescence regime.[10a]

For **10**, the chemical shifts of the NH^1 and NH^2 signals are displayed in Figure 4 as a function of the concentration of **21**. Implicit is that the equilibrium between the free and bound cyanurate is fast on the NMR time-scale. Nevertheless, overcoming the intermolecular hydrogen bonds (i.e., in **15** and **10**) takes time. Thus, to guarantee the establishment of a stable equilibrium, the ^{1}H NMR spectra were recorded 45 min after addition. The NMR titration plots for **10·21$_2$** and **15·21$_2$** gave rise to sigmoidal shapes with inflection points at around 0.6 equiv., which confirms an overall positive cooperativity.[31–33] Nevertheless, the cooperativity is affected by the nature of the dendron (see Figures 6 and 7), with **10·21$_2$** > **15·21$_2$**. The NMR assays for the first-generation dendron **20** revealed the most pronounced downfield shifts, reflecting the higher association constants (Table 1).

Table 1. Association constants, R factor (R), r_{max} and Hill coefficients (n_H) for the 1:2 complexes of **10** and **15** with dendrons **21**, **22**, and **23**.

	$\log K_1$ [L mol^{-1}]	$\mathrm{Log}\,K_2$ [L mol^{-1}]	R [%]	r_{max}	n_H
10·21$_2$	3.42	8.14	0.48	0.88	0.79
10·22$_2$	4.02	7.80	0.30	0.53	0.35
10·23$_2$	3.80	7.27	0.46	0.41	0.26
15·21$_2$	4.31	8.97	0.38	0.86	0.75
15·22$_2$	4.67	8.78	0.56	0.60	0.43
15·23$_2$	4.14	8.11	0.45	0.61	0.44

Calculation of the association constants (Table 1) was performed with the Chem-Equi program.[34,35] These calculations were based on assuming two equilibria [Equations (1) and (2)], namely between ZnP **10** and **15**[36] (C) and the depsipeptide dendrons **21**, **22**, and **23** (L).

$$K_1 = \mathbf{C} + \mathbf{L} \rightleftharpoons \mathbf{CL} \quad (1)$$

$$K_2 = \mathbf{CL} + \mathbf{L} \rightleftharpoons \mathbf{CL_2} \quad (2)$$

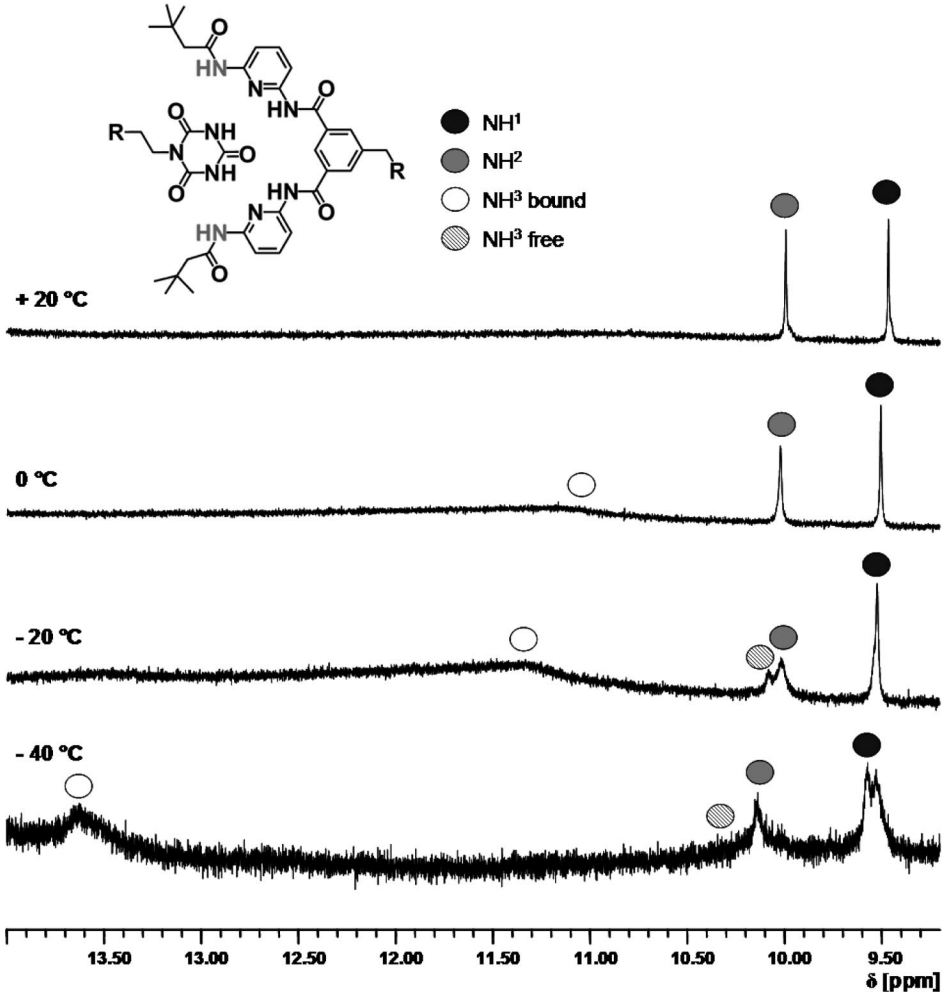

Figure 5. ^{1}H NMR spectra (400 MHz, $CDCl_3$) of a 1:8 mixture of **10** and **21** at various temperatures.

If identical and independent binding sites are considered, multiple binding proceeds under statistical conditions and, in turn, Equation (3) becomes relevant (t = total number of binding sites, $t = 2$).

$$\frac{K_{n+1}}{K_n} = \frac{n(t-n)}{(n+1)(t-n+1)} \quad (3)$$

Positive cooperativity leads us to expect higher binding strength of the (n+1)st ligand – relative to a statistical distribution – and higher K_{n+1}/K_n values.[29] Remarkably, the experimental K_{n+1}/K_n values were found to be even higher than those estimated on the basis of Equation (3). In all the cases $K_{n+1}/K_n > 1$, which clearly demonstrates the pronounced positive cooperativity for the supramolecular C/L_2 complexes.[37]

In light of the steric aspects, the association constants for **15**·$\mathbf{L}_2$ were higher than those for **10**·$\mathbf{L}_2$ (**L** = **21**, **22**, and **23**). The large difference between K_1 and K_2 reflects the pronounced positive cooperativity for these systems. The aforementioned tendency is inversely proportional to the generation number. In general, the association constants for the second binding decrease with increasing generation number of the depsipeptide dendrons **21**, **22**, and **23**. However, the K_1 values obtained for the second-generation dendrons **22** prevail over those of the self-assemblies involving the first-generation dendrons **21**. A different spatial arrangement is likely to be responsible for this trend. For example, open-chain Hamilton receptors such as **10** or **15** may adopt three different conformations depending on the degree of intermolecular aggregation and complexation. Only the *cis*/*cis* configuration ensures an effective complexation.[21] Binding of the first depsipeptide dendron weakens intermolecular aggregation and, in turn, facilitates binding of the second depsipeptide dendron. This trend scales with the generation number and the steric loading of the depsipeptide dendron. Importantly, the latter is also seen to decrease K_1.

All of the self-assembly processes feature dynamic character (see also Figure 5) and, as a consequence, the presence of three different species has to be assumed. Despite this, successful formation of the 1:2 complexes **C**·$\mathbf{L}_n$ (**C** = **10** or

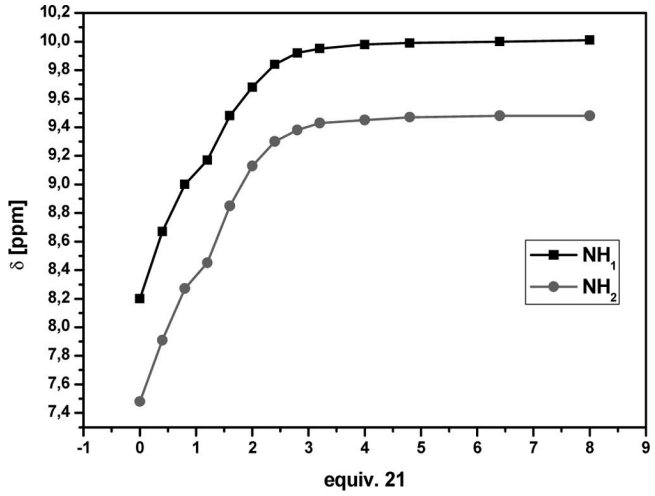

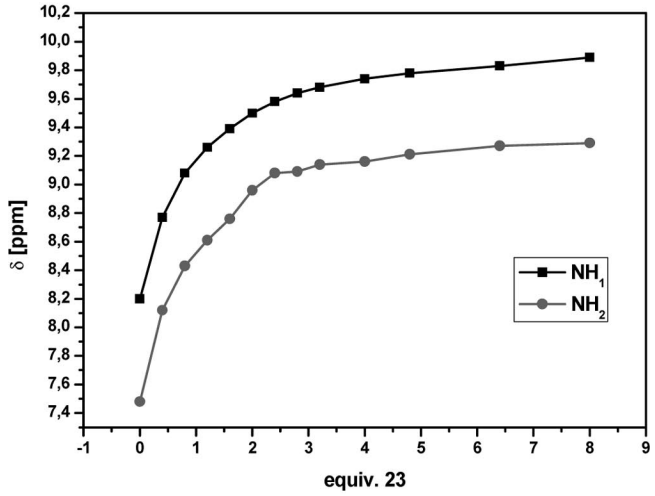

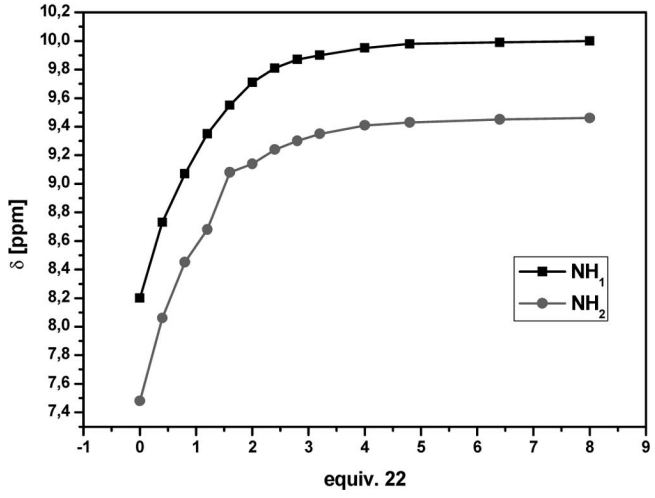

Figure 6. NMR titration reflecting the chemical shifts of NH^1 and NH^2 in **10** as a function of added equivalents of **21**, **22**, and **23**.

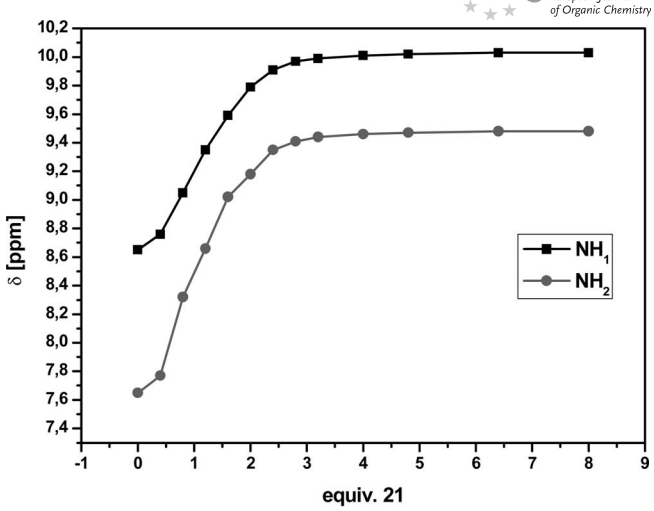

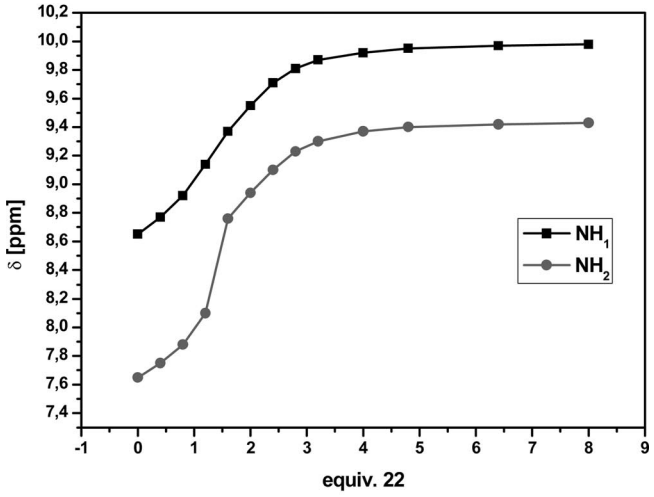

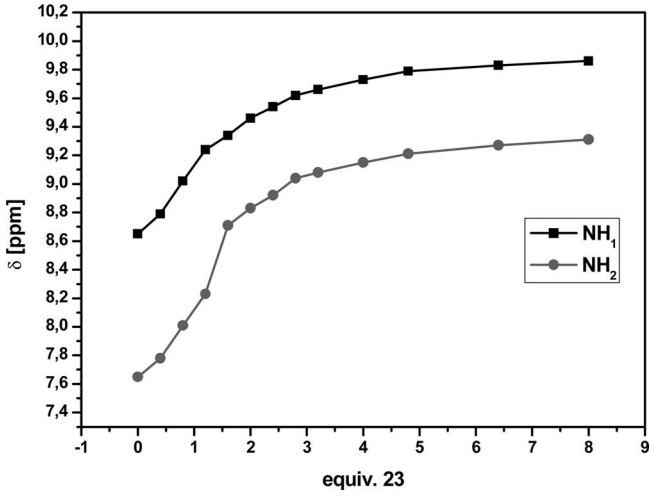

Figure 7. NMR titration reflecting the chemical shifts of NH^1 and NH^2 in **15** as a function of added equivalents of **21**, **22**, and **23**.

15; n = 0–2; **L** = **21**, **22** and **23**) is shown in Figures 8 and 9. Even at low concentrations of **21**, **22**, and **23** the $\mathbf{C{\cdot}L_2}$ complexes dominate, which guarantees that, upon addition of 2 equiv., the $\mathbf{C{\cdot}L_2}$ complexes range between 45–90%. The only exception is **23**, where the **C·L** complexes prevail until 1.6 or more equivalents have been added. Interestingly, the *cis* configuration in **10** evokes increased steric loadings. As a matter of fact, in the presence of 2 equiv. of **23**, the concentration of $\mathbf{15{\cdot}23_2}$ is close to 70%, whereas that of $\mathbf{10{\cdot}23_2}$ is only 45%.

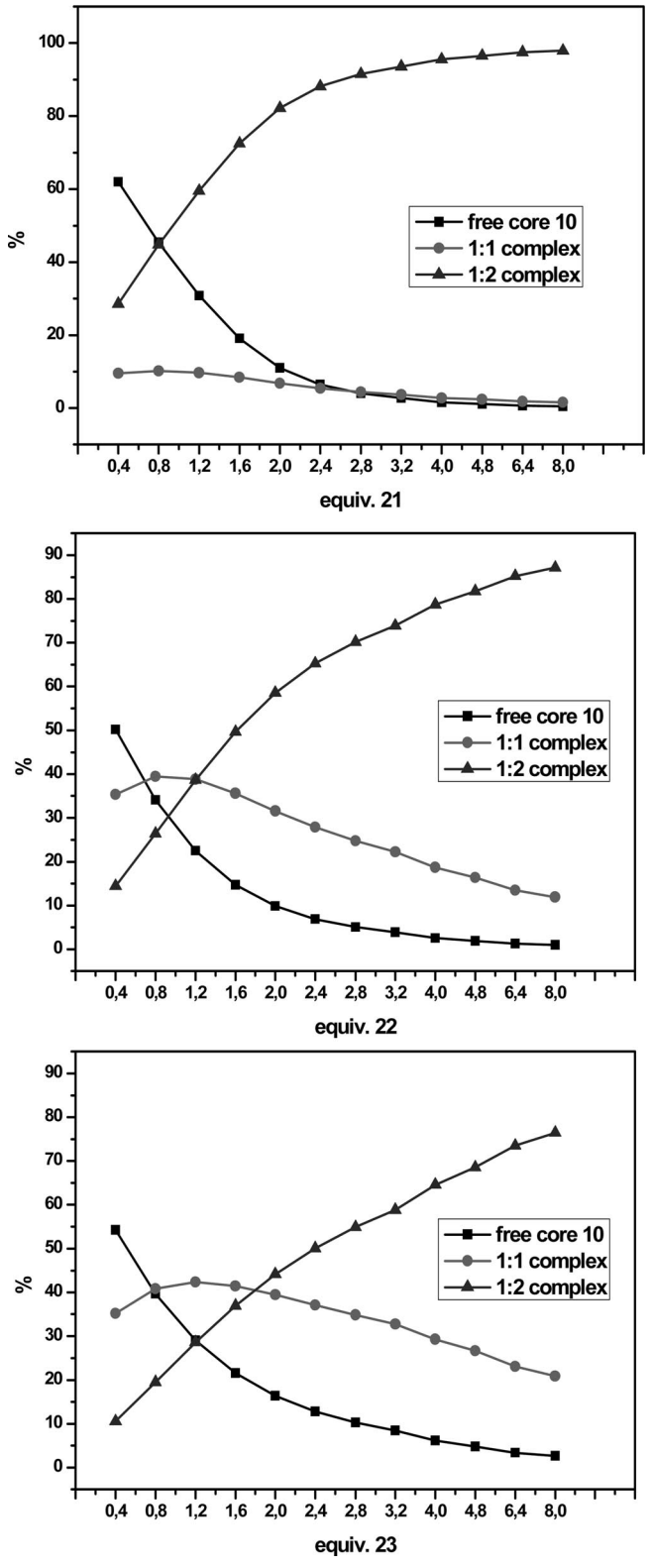

Figure 8. Distribution of free and complexed **10** in **10**·$\mathbf{L}_n$ (n = 0–2; **L** = **21**, **22**, and **23**) as a function of added equivalents of dendrons **21**, **22**, and **23**. The data was obtained from NMR analysis of the corresponding titrations by using Chem-Equi.[34,35]

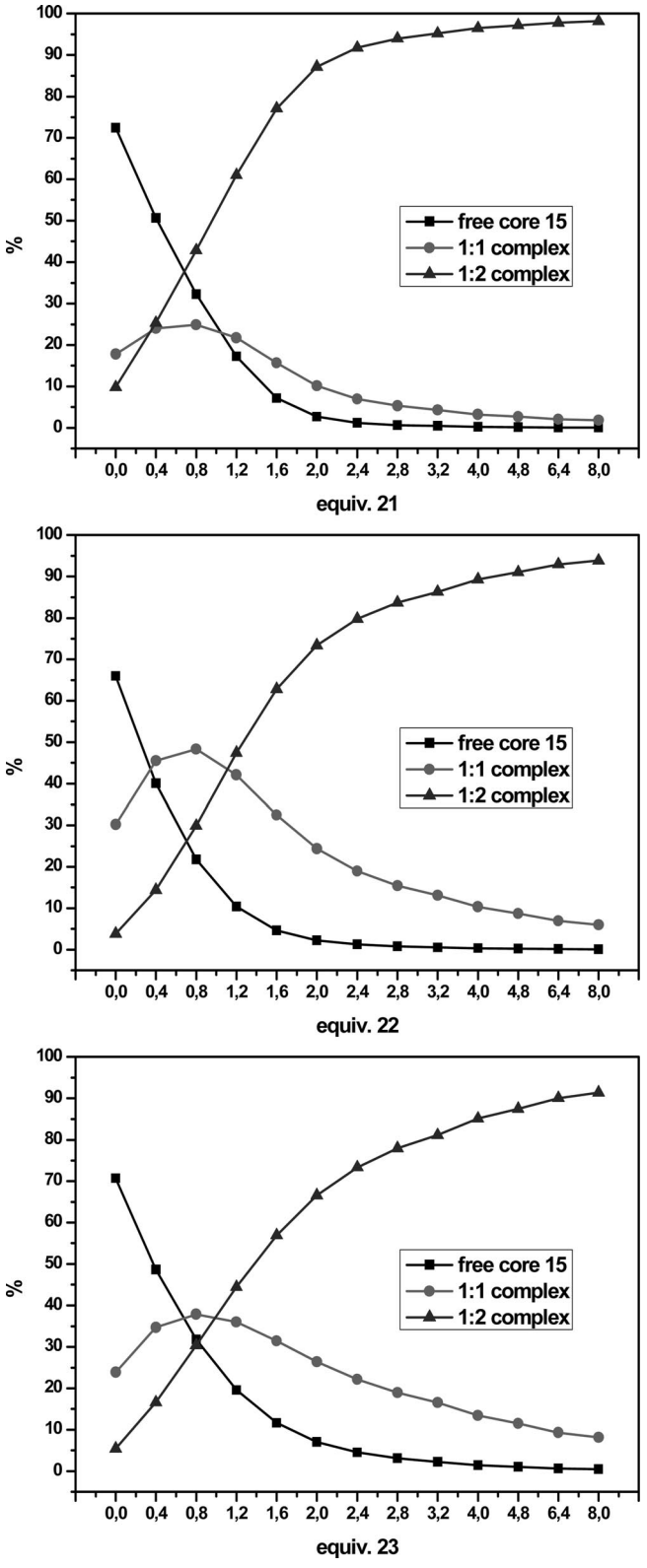

Figure 9. Distribution of free and complexed **15** in **15**·$\mathbf{L}_n$ (n = 0–2; **L** = **21**, **22**, and **23**) as a function of added equivalents of dendrons **21**, **22**, and **23**. The data was obtained from NMR analysis of the corresponding titrations by using Chem-Equi.[34,35]

Further confirmation for the positive cooperativity was obtained from the Scatchard[38] plots of the **C**·$\mathbf{L}_2$ systems (i.e., **C** = **10** or **15**; **L** = **21**, **22**, and **23**). Initially, the occupancy r as a reflection of the number of bound ligands was

determined from Equation (4) prior to analyzing the Scatchard Equation (5).

$$r = \frac{tQx}{(1 + Qx)} \quad (4)$$

$$r = \frac{[\mathbf{CL}] + 2[\mathbf{CL_2}]}{[\mathbf{C}] + [\mathbf{CL}] + [\mathbf{CL_2}]} \quad (5)$$

Assuming a statistical binding, the binding polynomial and r equal $(1 + Qx)^t$ and $tQx(1 + Qx)^{t-1}$, respectively. Here, x refers to the concentration of **L**.

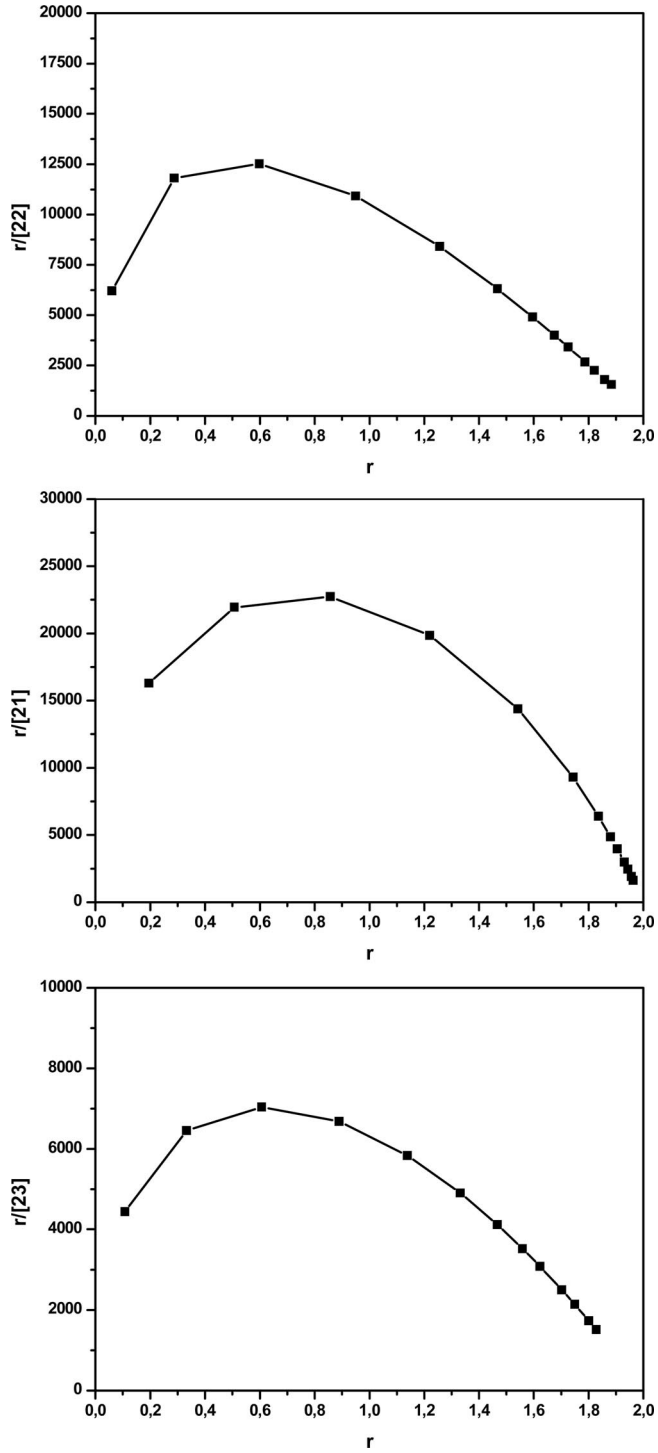

Figure 10. Scatchard plots for **15·L$_2$** (**L** = **21**, **22**, and **23**).

Figure 10 shows leading Scatchard plots. In all cases the plots feature convex curves, which points to pronounced positive cooperativity. Notably, statistical binding would result in a straight line, whereas concave Scatchard plots would suggest pronounced negative cooperativity.[29] A sizeable measure of the cooperativity is expressed by the Hill constants n_H,[39] which were determined from the maxima of the Scatchard plots r_{max} by using Equation (6).

$$n_H = \frac{r_{max}}{t - r_{max}} \quad (6)$$

In fact, the largest n_H values (Table 1) were associated with the formation of the **C·L$_2$** complexes when the first-generation dendron **21** was probed. Increasing the generation number of the dendron leads to smaller n_H values.

Finally, Job's plot analysis was performed with ^{1}H NMR titration data (see Figures 11 and 12) for the **C·L$_2$** systems (i.e., **C** = **10** and **L** = **22**; **C** = **15** and **L** = **21**). Overall, the obtained Job's plots give rise to maxima at a mol fraction of 0.33, which confirms the underlying 1:2 stoichiometry.

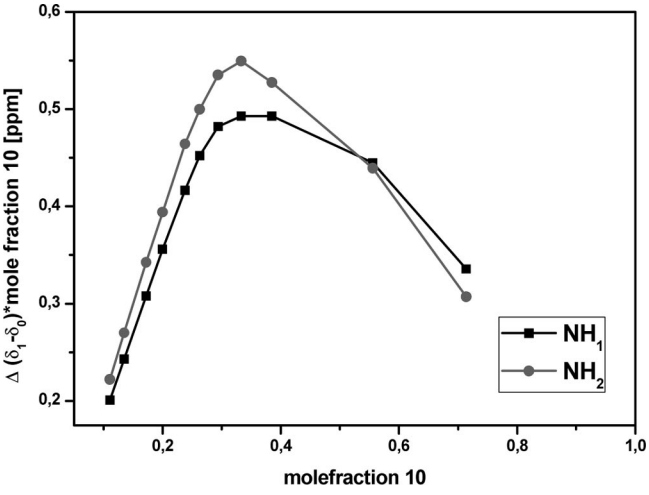

Figure 11. Job's plot analysis of the ^{1}H NMR titration of **10** with **22** in $CDCl_3$.

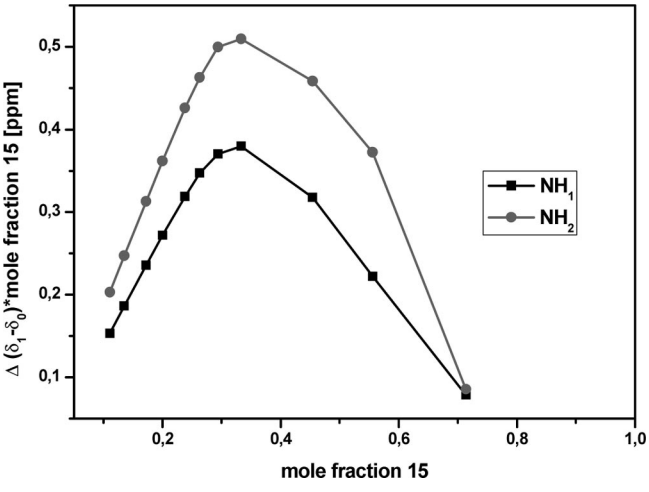

Figure 12. Job's plot analysis of the ^{1}H NMR titration of **15** with **21** in $CDCl_3$.

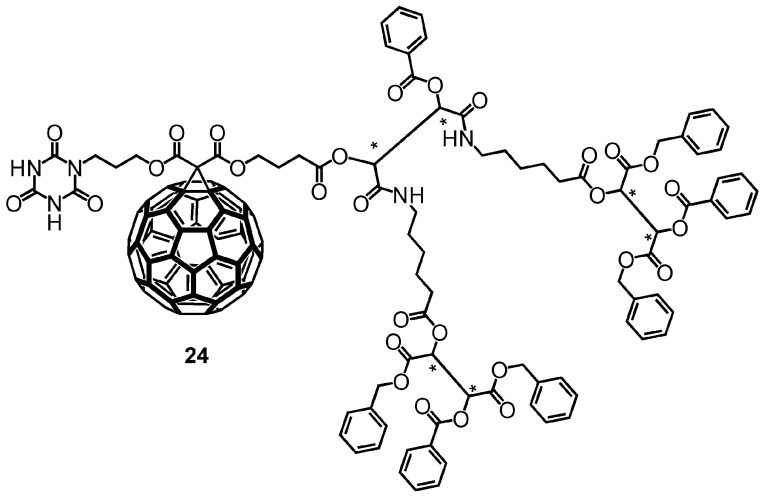

Figure 13. Depsipeptide fullerene **24** with all-(*S*) configuration.

Photophysical Investigations

As a complement, Zn–porphyrins **10**, **15**, and fullerene derivatives **20** and **24** (Figure 13) were subjected to a series of photophysical investigations.

To this end, solutions of Zn–porphyrin **10** (in dichloromethane, or *ortho*-dichlorobenzene) were titrated with variable concentrations of fullerene derivative **24**. We note – in perfect agreement with previous investigation – that adding **24** to solutions of **10** evoked a gradual redshift of the absorption features. For example, the Soret band shifts as much as 3 nm (see Figure 14). Moreover, when subtracting the fullerene absorption, a net decrease in the intensity of the Soret and Q-bands evolves. The presence of isosbestic points (418 and 428 nm) implies effective ground-state interactions between the Zn–porphyrin and fullerene.[40] A newly developing absorption band at 780 nm further corroborates this assumption.

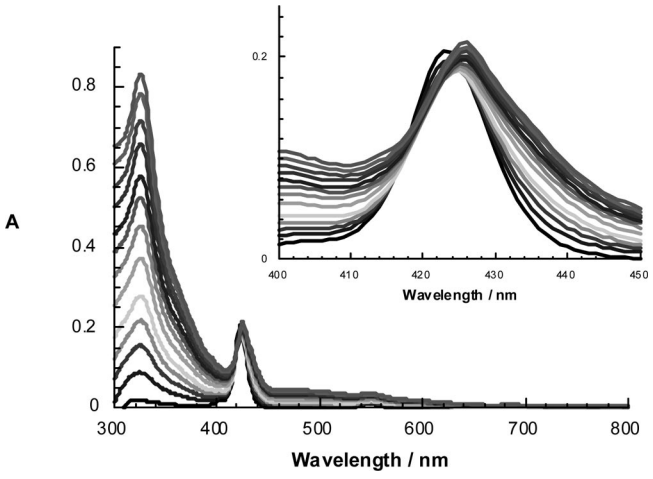

Figure 14. Changes in the Zn–porphyrin electronic absorption spectra of **10** (9.0×10^{-7} M) in CH_2Cl_2 upon successive addition of **24** (0 to 2.0×10^{-5} M).

With the changes in the absorption features in hand, we then quantified the binding constants. Considering the data at 423 nm (where the absorption diminishes) as a function of concentration of **24**, led to log*K* values of 3.30 L mol^{-1} and 6.71 L mol^{-1} for the first and second binding events, respectively.[41] Of note is the excellent agreement with the calculated values that were obtained based on the NMR titrations. Decisive information on the stoichiometry was obtained by Job's plot titration experiments. Figure 15 illustrates that the maximum occurs at 0.33, which points to a 1:2 stoichiometry.

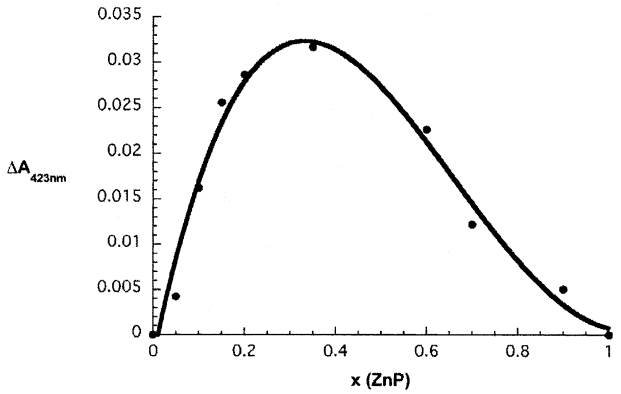

Figure 15. Job's plot analysis of the absorption titration of **10** with **24** in CH_2Cl_2.

In contrast, titrations involving Zn–porphyrin **15** and fullerene **24** in *ortho*-dichlorobenzene/pyridine (1000:1) revealed only a slight decrease of the Soret-band and no appreciable shift. A reasonable assumption can be made that – in addition to axial coordination – weaker binding in the presence of pyridine occurs. Nevertheless, the isosbestic points at 430 and 440 nm provided evidence for mutually interacting Zn–porphyrin **15** and fullerene. A similar conclusion can be derived for Zn–porphyrin **10** and fullerene derivative **20** in chloroform/carbon disulfide (5:1). However,

including a *p*-phenyleneethynylene spacer hampers sizeable ground-state interactions.[42]

Decisive confirmation on the nature of the electron donor–acceptor interactions came from complementary steady-state fluorescence experiments. Here, the characteristic fluorescence of Zn–porphyrin **10** (Φ_F = 0.04) was used and monitored while adding variable amounts of fullerene **24**. As shown in Figure 16, the Zn–porphyrin fluorescence is subjected to strong quenching when **24** is present. Tentatively, we invoke for this new deactivation pathway an electron transfer that evolves from the photoexcited Zn–porphyrin. Spectroscopic evidence in favor of the electron-transfer hypothesis came from transient absorption measurements (see below). The gradual quenching was used to estimate the binding constants (Figure 16b).

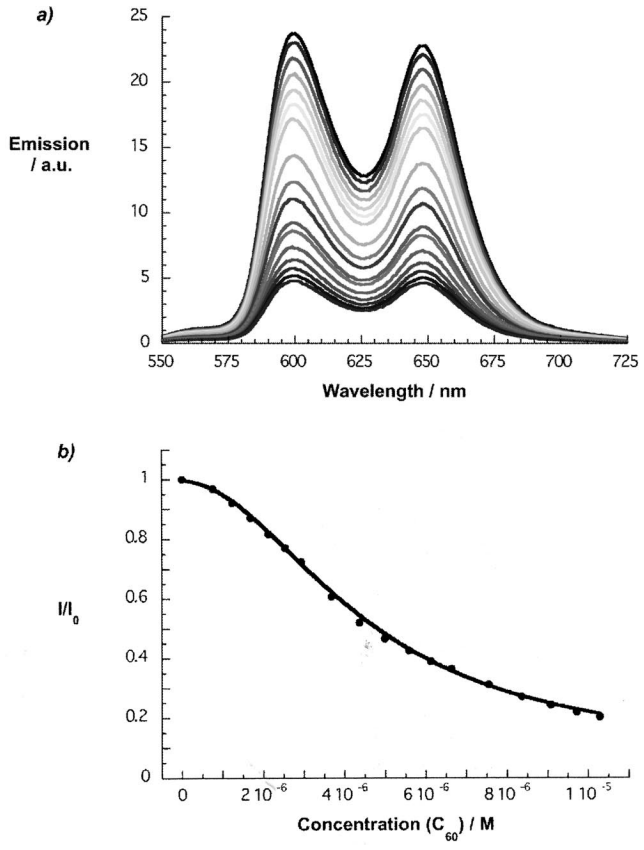

Figure 16. (a) Changes in the steady-state fluorescence of Zn–porphyrin **10** (8×10^{-7} M) upon successive addition of **24** (0 to 1.02×10^{-5} M) in *ortho*-dichlorobenzene; λ_{exc} = 424 nm. (b) Fluorescence intensity at 600 nm of **15** and **15·24** with non-linear fit according to Equation (7).

Using the sigmoidal dependency between I_F/I_0 and C_{60} concentration described by Equation (7) led to binding constants $\log K_1$ = 3.37 L mol^{-1} and $\log K_2$ = 7.30 L mol^{-1}.

$$I_F = \frac{(I_0 + c_0 \cdot b \cdot K_1 \cdot c_D + I_\infty \cdot \beta_{12} \cdot c_D^2)}{(1 + K_1 \cdot c_0 + \beta_{12} \cdot c_D^2)} \quad (7)$$

In Equation (7), I_0 and I_∞ refer to the initial and the final fluorescence intensity, respectively, whereas c_0 is the total porphyrin concentration; the added fullerene concentration is given by c_D. K_1 is the first binding constant and β_{12} equals $K_1 \cdot K_2$.[43] The perfect agreement with the NMR analysis and absorption assays strengthens our hypothesis for positive cooperativity.

An important control experiment focused on the non-photoactive dendron **22**,[10a] which was added in variable amounts to a mixture of **10** and **24** in *ortho*-dichlorobenzene. Upon increasing the concentration of **22** a ligand-exchange reaction replaced **24**, and the initial fluorescence of **10** was quantitatively restored.

The Zn–porphyrin fluorescence also enabled a determination of the extent of electronic communication between Zn–porphyrin **15** and **24**: $\log K_1$ = 3.92 L mol^{-1} and $\log K_2$ = 5.80 L mol^{-1} (Table 2). Interestingly, the difference between these two binding constants was much less when compared with the difference observed for **10·24**. A weaker cooperativity might arise from the *trans* positioning of the two Hamilton receptors.

In the next step, the fluorescence quantum yields at the plateau values – corresponding to a quantitative conversion – were taken to gather preliminary information about the excited-state deactivation dynamics. In **10·24**, for example, the new deactivation pathway (7.6×10^9 s^{-1}) outperforms the intrinsic decay of the singlet excited state of **10**, namely intersystem crossing (4.7×10^8 s^1).

Once the steady-state characterization – absorption and fluorescence – was completed, we turned to time-resolved fluorescence measurements. The fluorescence of Zn–porphyrin **10** was best fitted by a mono-exponential decay function with a lifetime that typically ranged from 1.5 to 1.8 ns, when dichloromethane and *ortho*-dichlorobenzene were used as solvents. In the presence of **24**, a reasonable fit of the fluorescence decay was only achieved when a bi-exponential fitting function was used. In particular, a long lifetime of ca. 1.5 ns – corresponding to free, uncomplexed **10** – and a short lifetime of 0.4 ns – corresponding to complexed **10·24** – emerged. The pre-exponential factor of the long and the short lifetimes decreased and increased with increasing concentration of **24**, respectively. Importantly,

Table 2. Association constants obtained from fluorescence titration for the 1:2 complexes of **10** and **15** with fullerene derivative **24** and fluorescence lifetimes of **10·24**.

	$\log K_1$ [L mol^{-1}]	$\log K_2$ [L mol^{-1}]	Fluorescence lifetime [τ] **10·24** [ns]	Solvent
10·24	3.54	6.37	1.6:0.4	dichloromethane
10·24	3.37	7.30	1.8:0.3	*ortho*-dichlorobenzene
15·24	3.92	5.80		*ortho*-dichlorobenzene/pyridine (1000:1)

the two lifetimes remained unchanged. From the short decaying component – attributed to complexed **10·24** – the rate of excited-state deactivation was estimated to be 2.8×10^9 s^{-1}. This is in good agreement with the deactivation rate obtained from the steady-state fluorescence experiments (7.6×10^9 s^{-1}). In a control experiment, redox- and photoinactive **22** was added to **10·24**. In this case, the pre-exponential factors were completely reverted, namely the short-lived component decreased gradually and finally disappeared, while that of the long-lived component increased likewise (Figure 17).

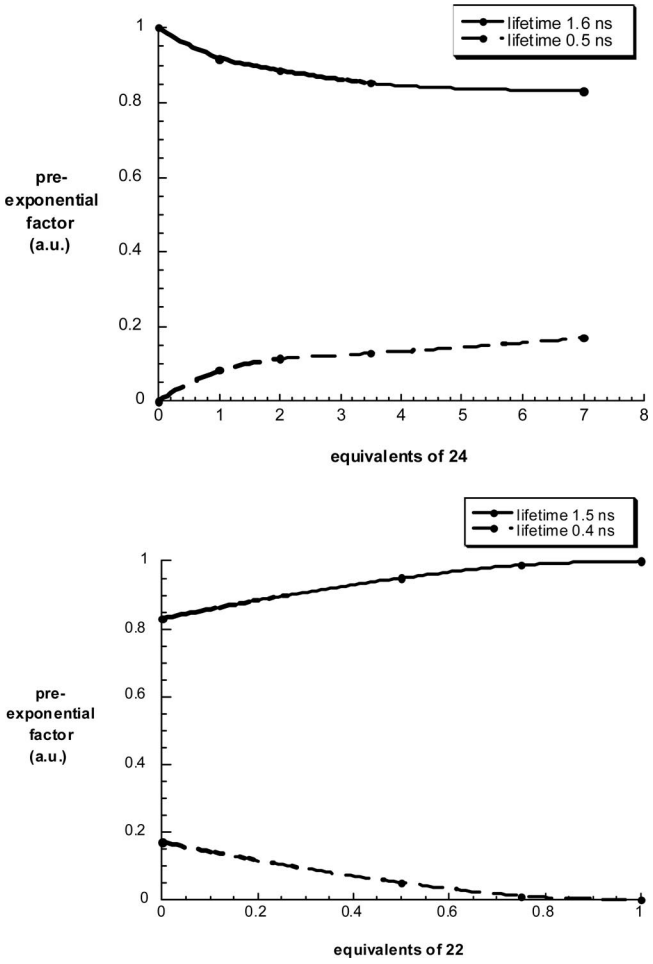

Figure 17. Normalized pre-exponential factors of the two lifetimes observed by time-correlated single-photon counting (TCSPC) as a function of the number of equivalents of fullerene **24** and dendron **22**.

Finally, we turned to transient absorption measurements to find spectroscopic and kinetic evidence in support of the hypothesized electron transfer. Representative femtosecond transient absorption spectra, recorded after a 150 fs laser pulse at 420 nm in *ortho*-dichlorobenzene solutions of **24**, are displayed in Figure 18. The spectra, obtained at time delays shortly after the laser pulse, revealed broadly absorbing features between 600 and 1100 nm. Superimposed onto that are features of transient bleach, especially around 420 and 550 nm. The latter features correspond to the loss of ground-state absorption. The singlet excited state ($E_{Singlet}$ = 2.0 eV) decays slowly (4.8×10^8 s^{-1}) to the energetically low-lying triplet excited state ($E_{Triplet}$ = 1.53 eV) through intersystem crossing ($\Phi_{Triplet}$ = 0.88). In terms of spectral characteristics of the latter, a maximum at around 840 nm should be considered.

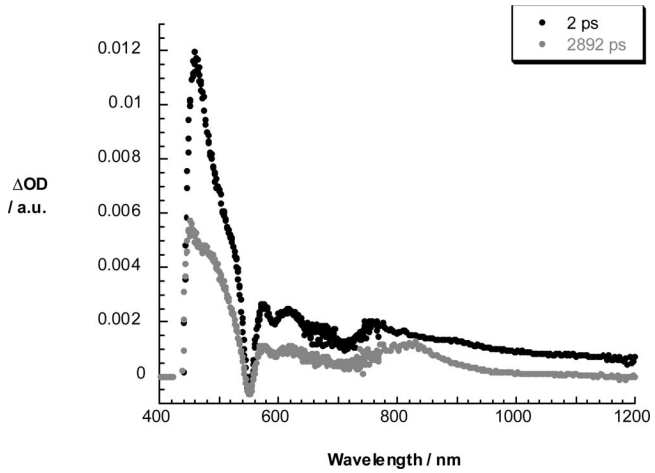

Figure 18. Differential absorption spectrum obtained upon femtosecond flash photolysis (420 nm) of zinc–porphyrin **24** in argon-saturated *ortho*-dichlorobenzene with time delays of 2 and 2892 ps.

Next, transient absorption measurements were carried out with **24·10**, and the results were compared with the spectra of **24**. At early time delays, transient absorption spectra of **24·10** were practically identical with those of **24**. However, at time delays of 100 ps the fingerprint absorptions of the one-electron-oxidized Zn–porphyrin radical cation and of the one-electron-reduced fullerene radical anion appeared at 680 and 1030 nm,[44] respectively. These radical ion pair features decayed over a time period of 3 ns to recover quantitatively the singlet ground state without populating any triplet excited states. In summary, electron transfer is responsible for the fast deactivation of the photoexcited Zn–porphyrin and, in turn, affords the formation of the radical ion pair state. By analyzing the kinetics of the time absorption profiles, we can derive rate constants for the charge separation and the charge recombination of 9.0×10^9 s^{-1} and 7.8×10^8 s^{-1}, respectively. Notably good is the agreement between the charge separation rate determined from steady-state fluorescence (7.6×10^9 s^{-1}) and transient absorption (9.0×10^9 s^{-1}) measurements (Figure 19).

Complementary nanosecond transient measurements, which were performed with 532 nm laser excitation of different mixtures of **24·10**, shed further light on the electron-transfer process. All the spectra were characterized by strong triplet–triplet absorptions at 710 nm, which correspond to that of the fullerene triplet excited state, without, however, giving rise to any radical ion pair features at 680 or at 1030 nm. We must assume that the fullerene triplet excited state originates from a locally excited state of free, uncomplexed fullerene. Implicit in this analysis is that in the femtosecond experiments, charge recombination occurs on a time-scale faster than in the nanosecond experiments, that is, less than 6 ns.

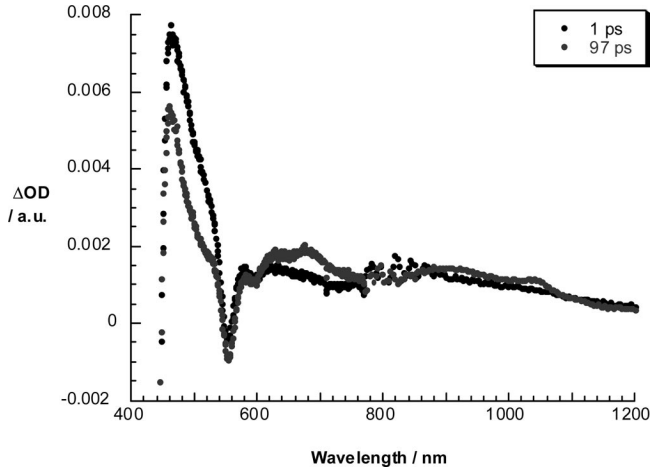

Figure 19. Differential absorption changes obtained upon femtosecond flash photolysis (420 nm) of **24·10** in argon-saturated *ortho*-dichlorobenzene with time delays of 1 and 97 ps.

Conclusions

We have investigated the aggregation and photophysical properties of supramolecular self-assemblies between *cis*- and *trans*-configured Hamilton receptor functionalized Zn–porphyrins and chiral depsipeptide (fullerene) cyanurates based upon the Hamilton receptor bonding motif. The corresponding association constants were determined by means of NMR and fluorescence titration experiments. In general, NMR titration analysis confirmed the largest complex stability, and most pronounced cooperativity for the 1:2 aggregates involved the first-generation depsipeptide dendron **21**; this was reflected in the values of the first and second binding steps (K_1 and K_2) and the Hill constant (n_H). The self-assembly of the supramolecular first- to third-generation complexes with *trans* geometry was found to be much more pronounced compared to their *cis*-substituted analogues. Furthermore, the association constants K_2 were found to decline with increasing generation number of the depsipeptide dendrons **21**, **22**, and **23** due to increased steric loading of the ligands. The graphical interpretations of all the possible **C·21**$_n$ complexes (**C** = **10** or **15**; n = 1–2) in solution as a function of the concentration of **21** revealed that the **C·21**$_2$ complexes prevail over the **C·21**$_1$ aggregates even at low concentrations. The formation of the **C·L**$_2$ assemblies involving the more bulky third-generation dendron **23** were found to be much less pronounced, and the percentage of the **C·23**$_2$ complex reached only 45–70%, whereas the concentration of the **C·21**$_2$ species varied between 95 and 100%. The 1:2 stoichiometry of the supramolecular first- to third-generation aggregates was confirmed by Job's plot analysis on the collected data from the ^{1}H NMR titration experiments. As a complement, supramolecular aggregates consisting of the Hamilton receptor functionalized Zn–porphyrins **10** or **15** with fullerene derivatives **20** or **24** as ligands were subjected to a series of photophysical investigations. Fluorescence titrations of solutions of Zn–porphyrin **10** (in CH_2Cl_2 or *ortho*-dichlorobenzene) with variable concentrations of fullerene derivative **24** allowed the association constants to be calculated; these were in excellent agreement with the estimated values based upon ^{1}H NMR titration analysis. In contrast to these outcomes, the self-assembly between Zn–porphyrin **15** and fullerene derivative **24** (*ortho*-dichlorbenzene/pyridine, 1000:1) was found to be much less pronounced. We believe that, in addition to intermolecular aggregation (axial coordination through the Zn^{2+} ion), weaker binding in the presence of pyridine can be considered to be a reasonable assumption. A similar conclusion can be reached for the self-assembly between Zn–porphyrin **10** and fullerene derivative **20** in a mixture of $CHCl_3$/carbon disulfide (5:1). A series of photophysical experiments – ranging from steady-state and time-resolved fluorescence experiments to transient absorption measurements on the femtosecond and nanosecond time-scales – provided decisive confirmation of the nature of electron donor–acceptor interactions because they are operative between Zn–porphyrin **10** and fullerene derivative **24** in the supramolecular assembly **24·10**.

Experimental Section

General Remarks: Commercially available chemicals were purchased from Aldrich, Fluka, Sigma, or Acros Organics. Compounds **1**, **2**, **3**, **11**, and **17** were synthesized according to literature procedures.[19–21,23,25] The preparation of chiral depsipeptide dendrons **21**–**23** and the fullerene derivative **20** was described previously.[10a,16] Solvents were dried by using standard techniques, anhydrous DMF was obtained from Acros. HPLC-grade solvents were purchased from Acros Organics or SDS. HPLC-grade $CHCl_3$ was freshly distilled from potassium carbonate (K_2CO_3) prior to use, to avoid protonation of the porphyrins **10** and **15**. For the same reason, $CDCl_3$ was stirred with K_2CO_3 and filtered prior to use. Reactions were monitored by thin-layer chromatography (TLC) using Riedel-de-Haën silica gel 60 F_{254} aluminum foil, detection at 254 nm by UV lamp. ^{1}H and ^{13}C NMR spectra were recorded with JEOL JNM EX 400, JEOL JNM GX 400, JEOL A 500, Bruker Avance 300, or Bruker Avance 400 spectrometers. The chemical shifts are given in ppm relative to tetramethylsilane (TMS) or to the solvent peak as a standard reference. The resonance multiplicities are indicated as: s (singlet), d (doublet), t (triplet), q (quartet), and m (multiplet), unresolved signals as broad (br.) or very broad (v. br.). Mass spectra were measured with a Micromass Lab Spec (FAB) using a Finnigan MAT 900 spectrometer with 3-nitrobenzyl alcohol as a matrix. IR spectra were recorded with a Bruker Vector 22 instrument with an ATR/RFS 100/S detector using liquid or powder substances. MALDI TOF mass spectra were measured with a Shimadzu Axima Confidence spectrometer (Version 3.04, Kratos Analytical) using 2,5-dihydroxybenzoic acid (DHTB), sinapinic acid (SIN), dithranol (DIT) or *trans*-2-[3-(4-*tert*-butylphenyl)-2-methyl-2-propynylidene]malononitrile (DCTB) as matrices. UV/Vis spectroscopy was performed by using a Specord S 600 spectrophotometer. Elementary analyses were performed by combustion and gas chromatographic analysis with an EA 1110 CHNS analyzer (CEInstruments). Products were isolated by flash column chromatography (FC) (silica gel 60, particle size 0.04–0.063 nm, Merck).

Synthesis of Compound 7: TFA (0.20 mL, 3.00 mmol) was added to a solution of **6** (759.00 mg, 3.75 mmol), **5** (623.00 mg, 3.75 mmol) and pyrrole **4** (0.50 mL, 7.50 mmol) in CH_2Cl_2 (150 mL). The reac-

tion mixture was stirred at room temp. for 1 h. After neutralization with NEt_3 (0.55 mL, 3.95 mmol), DDQ (1.28 g, 5.63 mmol) was added, and the solution was stirred at room temp. for a further 2 h. The crude reaction mixture was concentrated and filtered through SiO_2 by using CH_2Cl_2/EtOAc (9:1) as eluent. The desired porphyrin compound was separated by repeated column chromatography [SiO_2; hexane/EtOAc (8:2), R_f = 0.42]. Yield: 144.00 mg (9%); dark-violet powder. ^{1}H NMR (300 MHz, $CDCl_3$, 25 °C): δ = –2.78 (br., 2 H, NH), 0.43 (s, 18 H, CH_3), 4.00 (12 H, OCH_3), 6.95 [t, $^3J_{H,H}$ = 2.1 Hz, 2 H, Bn], 7.44 (d, $^3J_{H,H}$ = 2.1 Hz, 4 H, Bn), 7.91 (d, $^3J_{H,H}$ = 8.1 Hz, 4 H, Bn), 8.21 (d, $^3J_{H,H}$ = 8.1 Hz, 4 H, Bn), 8.87 (br., 4 H, pyrrole), 9.00 (br., 4 H, pyrrole) ppm. ^{13}C NMR (75 MHz, $CDCl_3$, 25 °C): δ = 0.49 (CH_3), 56.04 (OCH_3), 96.01 (C≡C), 100.55 (Bn), 105.39 (C≡C), 114.26, 119.77, 120.46, 123.04, 130.78, 134.79, 142.81, 144.30, 159.27 (Bn) ppm. $C_{58}H_{54}N_4O_4Si_2$ (927.26): calcd. C 75.13, H 5.87, N 6.04; found C 72.29, H 4.80, N 5.83. MS (FAB): *m*/*z* = 927 $[M]^+$. UV/Vis (CH_2Cl_2): λ (ε) = 422 (377800), 516 (16900), 552 (7400), 590 (5300), 646 (3900 L mol^{-1} cm^{-1}) nm. IR (ATR): $\tilde{\nu}_{max}$ = 3002, 2970, 2360, 2342, 2157, 1738, 1591, 1558, 1499, 1456, 1421, 1397, 1356, 1249, 1228, 1217, 1204, 1155, 1064, 1021, 974, 930, 859, 800, 762, 735 cm^{-1}.

Synthesis of Compound 8: $Zn(OAc)_2$ dihydrate (72.00 mg, 330.00 μmol) was added to a solution of **7** (60.00 mg, 66.60 μmol) in THF (15 mL). The reaction was mixture was heated at reflux for 90 min. The solution was concentrated to dryness and purified by column chromatography (SiO_2; CH_2Cl_2, R_f = 0.85). Yield: 79.00 mg (81%); pink powder. ^{1}H NMR (300 MHz, $CDCl_3$, 25 °C): δ = 0.39 (s, 18 H, CH_3), 3.91 (s, 12 H, OCH_3), 6.84 (t, $^3J_{H,H}$ = 2.1 Hz, 2 H, Bn), 7.36 (d, $^3J_{H,H}$ = 2.4 Hz, 4 H, Bn), 7.87 (d, $^3J_{H,H}$ = 8.1 Hz, 4 H, Bn), 8.16 (d, $^3J_{H,H}$ = 7.8 Hz, 4 H, Bn), 8.87 (m, 4 H, pyrrole), 9.00 (m, 4 H, pyrrole) ppm. ^{13}C NMR (75 MHz, $CDCl_3$, 25 °C): δ = 0.07 (CH_3), 55.58 (OCH_3), 95.38 (C≡C), 99.97 (Bn), 105.07 (C≡C), 113.69, 120.30, 120.96, 122.31, 130.21 (Bn), 131.70, 131.79, 132.10, 132.20 (pyrrole), 134.24, 143.09, 144.53 (Bn), 149.75, 149.86, 149.98, 150.09 (pyrrole), 158.64 (Bn) ppm. $C_{58}H_{52}N_4O_4Si_2Zn{\cdot}0.25CH_2Cl_2$ (1011.58): calcd. C 69.14, H 5.23, N 5.54; found C 69.17, H 5.56, N, 5.08. MS (FAB): *m*/*z* = 990 $[M]^+$. UV/Vis (CH_2Cl_2): λ (ε) = 423 (513500), 549 (20400), 588 (2900 L mol^{-1} cm^{-1}) nm. IR (ATR): $\tilde{\nu}_{max}$ = 3002, 2970, 2360, 2342, 2157, 1739, 1592, 1524, 1494, 1455, 1421, 1366, 1350, 1249, 1228, 1217, 1204, 1154, 1065, 1001, 950, 932, 859, 843, 811, 797, 760, 719 cm^{-1}.

Synthesis of Compound 9: A solution of TBAF in THF (1 M, 0.40 mL) was added dropwise to a solution of compound **8** (66.00 mg, 68.40 μmol) in anhydrous THF (5 mL). The reaction mixture was stirred under inert conditions at room temp. for 12 h. The solution was concentrated to dryness, the residue was dissolved in CH_2Cl_2 (15 mL) and extracted with aq. $NaHCO_3$ (5%; 2 × 10 mL). The organic layer was separated, washed with water (2 × 10 mL) and dried with Na_2SO_4. The solution was filtered, concentrated to dryness and purified by column chromatography (SiO_2; CH_2Cl_2, R_f = 0.66). Yield: 62.00 mg (93%); pink powder. ^{1}H NMR (300 MHz, $CDCl_3$, 25 °C): δ = 3.32 (s, 2 H, C≡H), 3.91 (s, 12 H, OCH_3), 6.85 (br., 2 H, Bn), 7.37 (d, $^3J_{H,H}$ = 2.1 Hz, 4 H, Bn), 7.88 (d, $^3J_{H,H}$ = 8.1 Hz, 4 H, Bn), 8.18 (d, $^3J_{H,H}$ = 8.1 Hz, 4 H, Bn), 8.92 (m, 4 H, pyrrole), 9.03 (m, 4 H, pyrrole) ppm. ^{13}C NMR (75 MHz, $CDCl_3$, 25 °C): δ = 55.58 (OCH_3), 87.16 (C≡CH), 83.72 (C≡C), 99.95, 113.73, 120.09, 120.98, 121.32, 130.36 (Bn), 131.68, 131.77, 132.11, 132.21 (pyrrole), 134.31, 143.47, 144.55 (Bn), 149.70, 149.83, 149.97, 150.11 (pyrrole), 158.62 (Bn) ppm. $C_{52}H_{36}N_4O_4Zn{\cdot}1.5C_6H_{14}$ (975.53): calcd. C 73.80, H 4.29, N 6.62, O 7.20, Zn 7.35; found C 74.89, H 5.95, N 5.51. MS (FAB): *m*/*z* = 844 $[M]^+$. UV/Vis (CH_2Cl_2): λ (ε) = 422 (502900), 549 (20900), 588 (3400 L mol^{-1} cm^{-1}) nm. IR (ATR): $\tilde{\nu}_{max}$ = 3287, 3004, 2970, 2360, 2341, 1738, 1591, 1525, 1494, 1455, 1421, 1366, 1348, 1229, 1216, 1203, 1154, 1065, 1001, 950, 933, 858, 811, 797, 767, 745, 719 cm^{-1}.

Synthesis of Compound 10: Compound **3** (73.60 mg, 110.00 μmol) was dissolved in anhydrous THF/NEt_3 (2:1, 12 mL). $Pd_2(dba)_3$ (77.00 mg, 84.10 μmol), $AsPh_3$ (129.00 mg, 421.00 μmol) and **9** (30.00 mg, 36.60 μmol) were added, and the reaction was allowed to proceed in the dark under inert conditions for 6 d. The solution was concentrated to dryness and purified by repeated column chromatography [SiO_2; CH_2Cl_2 → CH_2Cl_2/EtOAc (1:1), CH_2Cl_2/MeOH (99:1 → 98:2); R_f = 0.18 (CH_2Cl_2/EtOAc, 98:2)]. The dark-red powder was dissolved in CH_2Cl_2 and precipitated with *n*-pentane. Yield: 27.00 mg (38%); dark-violet powder. ^{1}H NMR (400 MHz, [D$_8$]THF, 25 °C): δ = 1.10 (s, 36 H, CH_3), 2.58 (s, 8 H, CH_2), 3.95 (s, 12 H, OCH_3), 6.93 (t, $^3J_{H,H}$ = 2.1 Hz, 2 H, Bn), 7.39 (d, $^3J_{H,H}$ = 2.4 Hz, 4 H, Bn), 7.76 (t, $^3J_{H,H}$ = 8.1 Hz, 4 H, Py), 8.07 (overl. m, 12 H, Bn, Py), 8.30 (d, $^3J_{H,H}$ = 8.1 Hz, 4 H, Py), 8.45 (d, $^3J_{H,H}$ = 1.8 Hz, 4 H, Bn), 8.55 (br.,2 H, Bn), 8.88–9.01 (overl. m, 8 H, pyrrole), 9.08 (br., 4 H, NH), 9.77 (br., 4 H, NH) ppm. ^{13}C NMR (100.5 MHz, $CDCl_3$, 25 °C): δ = 29.99 (CH_3), 31.64 (CCH_3), 50.71 (CH_2), 55.62 (OCH_3), 89.47, 91.67 (C=C), 98.63, 100.14 (Bn), 110.21, 110.42 (Py), 114.65, 120.30, 121.73, 122.55, 124.96, 127.53, 130.48 (Bn), 131.93, 132.38 (pyrrole), 134.29, 135.52, 136.80, 140.57, 145.29, 145.87 (Bn), 150.36, 150.60, 150.82, 151.01 (pyrrole), 151.23, 151.76, 159.86 (Bn), 164.88, 170.75 (C=O) ppm. $C_{112}H_{104}N_{16}O_{12}Zn{\cdot}1.5CH_2Cl_2$ (2058.91): calcd. C 66.21, H 5.24, Cl 5.17, N 10.86, O 9.32, Zn 3.18; found C 66.44, H 4.80, N 10.32. MS (FAB): *m*/*z* = 1932 $[M]^+$. UV/Vis (CH_2Cl_2): λ (ε) = 303 (127700), 424 (590700), 550 (26500), 589 (6400 L mol^{-1} cm^{-1}) nm. IR (ATR): $\tilde{\nu}_{max}$ = 3003, 2970, 2360, 2341, 1738, 1586, 1522, 1507, 1446, 1366, 1352, 1298, 1229, 1217, 1204, 1154, 1066, 999, 950, 904, 858, 797, 752, 719 cm^{-1}.

Synthesis of Compound 12: TFA (1.00 mL, 13.10 mmol) was added to a solution of **11** (3.00 g, 8.19 mmol) and 4-[2-(trimethylsilyl)ethynyl]benzaldehyde (**6**; 1.66 g, 8.19 mmol) in CH_2Cl_2 (655 mL). The reaction mixture was stirred at room temp. for 1 h. After neutralization with NEt_3 (2.40 mL, 17.03 mmol), DDQ (2.79 g, 12.28 mmol) was added, and the solution was stirred at room temp. for a further 2 h. The crude reaction mixture was concentrated and filtered through SiO_2 by using CH_2Cl_2/EtOAc (95:5) as eluent. The desired porphyrin isomer was separated by repeated column chromatography (SiO_2; CH_2Cl_2, R_f = 0.22). Yield: 448.00 mg (10%); violet powder. ^{1}H NMR (400 MHz, $CDCl_3$, 25 °C): δ = –2.67 (br., 2 H, pyrrole NH), 0.39 (s, 18 H, $SiCH_3$), 1.65 (s, 18 H, CH_3), 2.78 (s, 12 H, OCH_3), 3.93 (s, 8 H, CH_2), 7.89 (m, 8 H, Bn), 8.17 (d, $^3J_{H,H}$ = 8.4 Hz, 4 H, Bn), 8.70 (d, $^3J_{H,H}$ = 4.8 Hz, 4 H, pyrrole), 8.78 (d, $^3J_{H,H}$ = 4.8 Hz, 4 H, pyrrole) ppm. ^{13}C NMR (100.5 MHz, $CDCl_3$, 25 °C): δ = 0.47 ($SiCH_3$), 32.12 (CH_3), 35.65 (CCH_3), 58.51 (OCH_3), 73.45 (CH_2), 96.11, 105.34 (C≡C), 115.79, 119.56, 122.87, 123.08, 130.84, 134.87, 135.39, 139.93, 142.40, 152.46 (Bn) ppm. $C_{70}H_{78}N_4O_4Si_2{\cdot}1.5CH_2Cl_2$ (1166.86): calcd. C 69.48, H 6.31, Cl 9.12, N 4.80, O 5.48, Si 4.81; found C 69.51, H 7.40, N 4.65. MS (FAB): *m*/*z* = 1095 $[M]^+$. UV/Vis (CH_2Cl_2): λ (ε) = 422 (394500), 517 (17300), 552 (7300), 592 (5300), 647 (3800 L mol^{-1} cm^{-1}) nm. IR (ATR): $\tilde{\nu}_{max}$ = 2970, 2360, 2342, 2157, 1738, 1474, 1457, 1365, 1251, 1228, 1217, 1205, 1103, 1022, 981, 967, 862, 847, 802, 761, 741, 714 cm^{-1}.

Synthesis of Compound 13: $Zn(OAc)_2$ dihydrate (200.00 mg, 0.91 mmol) was suspended in MeOH (2 mL) and added to a solution of **12** (200.00 mg, 0.18 mmol) in THF (60 mL). The reaction mixture was heated at reflux for 12 h. The solution was concentrated to dryness and purified by column chromatography (SiO_2,

CH_2Cl_2/EtOAc, 9:1). Yield: 175.00 mg (83%); pink powder. ^{1}H NMR (400 MHz, $CDCl_3$/[D_5]pyridine, 25 °C): δ = 0.38 (s, 18 H, $SiCH_3$), 1.64 (s, 18 H, CH_3), 2.71 (s, 12 H, OCH_3), 3.88 (s, 8 H, CH_2), 7.84 (m, 8 H, Bn), 8.17 (d, $^3J_{H,H}$ = 8.0 Hz, 4 H, Bn), 8.66 (d, $^3J_{H,H}$ = 4.8 Hz, 4 H, pyrrole), 8.76 (d, $^3J_{H,H}$ = 4.8 Hz, 4 H, pyrrole) ppm. ^{13}C NMR (100.5 MHz, $CDCl_3$/[D_5]pyridine, 25 °C): δ = 0.50 ($SiCH_3$), 32.16 (CH_3), 35.59 (CCH_3), 58.33 (OCH_3), 73.52 (CH_2), 95.58, 105.68 (C≡C), 115.90, 119.81, 122.29, 122.49, 130.41 (Bn), 130.41, 131.32 (8 C, pyrrole), 132.28, 134.97, 136.83, 139.71, 144.07 (Bn), 150.16, 150.23 (pyrrole), 151.77 (Bn) ppm. $C_{70}H_{76}N_4O_4Si_2Zn{\cdot}0.5H_2O$ (1167.95): calcd. C 71.30, H 6.26, N 5.04, O 6.48, Zn 5.88; found C 71.60, H 6.55, N 5.32. MS (FAB): *m*/*z* = 1158 [M^+]. UV/Vis (CH_2Cl_2): λ (ε) = 423 (482500), 551 (21800), 589 (3200 L mol^{-1} cm^{-1}) nm. IR (ATR): $\tilde{\nu}_{max}$ = 2970, 2360, 2157, 1738, 1460, 1365, 1248, 1228, 1217, 1203, 1115, 996, 967, 858, 843, 797, 758, 721 cm^{-1}.

Synthesis of Compound 14: A solution of TBAF in THF (1 M, 0.86 mL) was added dropwise to a solution of **13** in anhydrous THF (10 mL). The reaction mixture was stirred under inert conditions at room temp. for 12 h. The solution was concentrated to dryness, and the residue was dissolved in CH_2Cl_2 (30 mL) and extracted with aq. $NaHCO_3$ (5%, 2 × 30 mL). The organic layer was separated, washed with water (2 × 30 mL) and dried with Na_2SO_4. The solution was filtered, concentrated to dryness and purified by column chromatography [SiO_2; CH_2Cl_2/EtOAc (97:3); R_f = 0.52]. Yield: 115.00 mg (79%); pink powder. ^{1}H NMR (400 MHz, $CDCl_3$/[D_5]pyridine, 25 °C): δ = 1.63 (s, 18 H, CH_3), 2.71 (s, 12 H, OCH_3), 3.33 (s, 2 H, C≡H), 3.88 (s, 8 H, CH_2), 7.84 (m, 8 H, Bn), 8.17 (d, $^3J_{H,H}$ = 8.0 Hz, 4 H, Bn), 8.67 (d, $^3J_{H,H}$ = 4.4 Hz, 4 H, pyrrole), 8.77 (d, $^3J_{H,H}$ = 4.4 Hz, 4 H, pyrrole) ppm. ^{13}C NMR (100.5 MHz, $CDCl_3$/[D_5]pyridine, 25 °C): δ = 32.16 (CH_3), 35.59 (CCH_3), 58.31 (OCH_3), 73.52 (CH_2), 78.47 (C≡C), 84.30 (C≡CH), 115.96, 119.69, 121.37, 122.52, 130.56 (Bn), 131.37, 132.30 (pyrrole), 135.01, 136.10, 136.84, 139.72, 144.36 (Bn), 150.13, 150.27 (pyrrole), 151.80 (Bn) ppm. MS (FAB): *m*/*z* = 1012 [$M]^+$. $C_{64}H_{60}N_4O_4Zn{\cdot}0.5H_2O$ (1023.59): calcd. C 74.49, H 5.52, N 5.79, O 7.44, Zn 6.76; found C 74.08, H 5.88, N 5.16. UV/Vis (CH_2Cl_2): λ (ε) = 423 (636200), 551 (20000), 588 (16600 L mol^{-1} cm^{-1}) nm. IR (ATR): $\tilde{\nu}_{max}$ = 3003, 2970, 2360, 2341, 1738, 1456, 1365, 1229, 1217, 1205, 1102, 1065, 998, 908, 809, 797, 720 cm^{-1}.

Synthesis of Compound 15: Compound **3** (87.20 mg, 130.04 μmol) was dissolved in anhydrous THF/NEt_3 (2:1, 17.5 mL). $Pd_2(dba)_3$ (114.20 mg, 124.71 μmol), $AsPh_3$ (191.40 mg, 625.02 μmol) and **14** (55.00 mg, 542.10 μmol) were added to this solution, and the reaction was allowed to proceed in the dark under inert conditions for 6 d. The solution was concentrated to dryness and purified by repeated column chromatography [SiO_2; CH_2Cl_2 → CH_2Cl_2/MeOH (99:1) → CH_2Cl_2/MeOH (98:2) → CH_2Cl_2/MeOH (98:5)]. The dark-red substance was dissolved in CH_2Cl_2 and precipitated with *n*-pentane. Yield: 35.00 mg (31%); violet powder. ^{1}H NMR (400 MHz, [D_8]THF, 25 °C): δ = 1.10 (s, 36 H, CH_3), 1.65 (s, 18 H, CH_3), 2.29 (s, 8 H, CH_2), 2.78 (s, 12 H, OCH_3), 3.95 (s, 8 H, CH_2), 7.77 (t, $^3J_{H,H}$ = 8.0 Hz, 4 H, Py), 7.94 (s, 4 H, Bn), 8.06 (overl. d, 20 H, Bn, Py), 8.29 (d, $^3J_{H,H}$ = 7.9 Hz, 4 H, Bn), 8.45 (s, 4 H, Bn), 8.57 (s, 2 H, Bn), 8.69 (d, $^3J_{H,H}$ = 4.5 Hz, 4 H, pyrrole), 8.84 (d, $^3J_{H,H}$ = 4.5 Hz, 4 H, pyrrole), 9.09 (br., 4 H, NH), 9.79 (br., 2 H, NH) ppm. ^{13}C NMR (100.5 MHz, [D_8]THF, 25 °C): δ = 30.00 (CH_3), 31.63 (CCH_3), 31.97 (CH_3), 35.70 (CCH_3), 50.71 (CH_2), 57.94 (OCH_3), 73.84 (CH_2), 89.51, 91.97 (C≡C), 110.20, 110.41 (Py), 116.52, 120.28, 122.54, 122.73, 124.95, 127.54, 130.44 (Bn), 131.39, 132.39 (pyrrole), 134.27, 135.68, 136.80 (Bn), 140.57 (Py), 145.03, 150.58, 150.67, 151.25 (Bn, Py), 151.66, 151.78 (pyrrole), 164.88, 170.77 (C=O) ppm. MALDI TOF/MS: *m*/*z* = 2736 [$M]^+$. $C_{124}H_{128}N_{16}O_{12}Zn{\cdot}2CH_2Cl_2$ (2213.59): calcd. C 66.20, H 5.65, Cl 6.41, N 10.12, O 8.67, Zn 2.95; found C 66.74, H 5.87, N 10.04. UV/Vis (CH_2Cl_2): λ (ε) = 303 (103400), 424 (432700), 552 (22800), 591 (5700 L mol^{-1} cm^{-1}) nm. IR (ATR): $\tilde{\nu}_{max}$ = 2970, 2360, 2342, 1738, 1586, 1523, 1447, 1366, 1299, 1230, 1217, 1205, 1154, 1118, 996, 889, 797, 720 cm^{-1}.

Synthesis of Compound 16: Nickel(II) acetylacetonate (29.31 mg, 114.10 μmol) was added to a solution of porphyrin **12** (25.00 mg, 22.82 μmol) in toluene (20.0 mL), and the reaction mixture was heated at reflux for 12 h. The solution was concentrated to dryness and purified by column chromatography [SiO_2; CH_2Cl_2/hexane (8:2); R_f = 0.46]. Yield: 21.0 mg (80%); cherry-red powder. ^{1}H NMR (400 MHz, $CDCl_3$, 25 °C): δ = 0.37 (s, 18 H, CH_3), 1.61 (s, 18 H, CH_3), 2.86 (s, 12 H, CH_3), 3.90 (s, 8 H, CH_2), 7.83 (m, 8 H, Bn), 8.02 (d, $^3J_{H,H}$ = 8.4 Hz, 4 H, Bn), 8.61 (d, $^3J_{H,H}$ = 5.2 Hz, 4 H, pyrrole), 8.70 (d, $^3J_{H,H}$ = 5.2 Hz, 4 H, pyrrole) ppm. ^{13}C NMR (100.5 MHz, $CDCl_3$, 25 °C): δ = 0.46, 32.09 (CH_3), 35.60 (CCH_3), 58.58 (CH_3), 73.29 (CH_2), 96.00, 105.30 (C≡C), 115.07, 118.72, 122.93, 123.12, 130.95 (Bn), 132.14, 123.69 (pyrrole), 134.03, 134.30, 139.53, 141.54, 143.16, 143.17, 152.40 (pyrrole, Bn) ppm. MALDI TOF/MS: *m*/*z* = 1150 [$M]^+$. $C_{70}H_{76}N_4NiO_4Si_2{\cdot}1.5CH_2Cl_2$ (1276.41): calcd. C 67.11, H 6.22, Cl 8.31, N 4.38, Ni 4.59, O 5.00, Si 4.39; found C 66.69, H 6.19, N 4.15. UV/Vis (CH_2Cl_2): λ (ε) = 417 (264200), 528 (20900 L mol^{-1} cm^{-1}) nm. IR (ATR): $\tilde{\nu}_{max}$ = 2961, 2924, 2822, 2159, 1605, 1499, 1393, 1351, 1290, 1250, 1220, 1194, 1102, 1003, 952, 930, 863, 843, 815, 803, 761, 716 cm^{-1}.

Synthesis of Compound 19: (4-Iodophenyl)isocyanuric acid (**17**; 150.00 mg, 0.45 mmol), $Pd(PPh_3)_2Cl_2$ (3.00 mg, 5.00 μmol) and CuI (3.00 mg, 15.00 μmol) were dissolved in THF (10 mL). To this solution, NEt_3 (4 mL) and 4-ethynylbenzaldehyde (**18**; 70.00 mg, 0.54 mmol) were added, and the reaction mixture was stirred at room temp. for 16 h. The precipitate was filtered off, the solvent was evaporated, and the crude product was purified by column chromatography [SiO_2; CH_2Cl_2 → CH_2Cl_2/THF (1:1)]. Yield: 110.00 mg (73%). ^{1}H NMR (400 MHz, [D_8]THF, 25 °C): δ = 7.17 (d, $^3J_{H,H}$ = 7.02 Hz, 2 H, Bn), 7.45 (d, $^3J_{H,H}$ = 8.5 Hz, 2 H, Bn), 7.80 (d, $^3J_{H,H}$ = 8.7 Hz, 2 H, Bn), 7.98 (d, $^3J_{H,H}$ = 6.7 Hz, 2 H, Bn), 10.93 (s, 1 H, HC=O), 11.59 (br., 2 H, NH) ppm. ^{13}C NMR (100.5 MHz, [D_8]THF, 25 °C): δ = 87.54, 90.56 (C≡C), 120.16, 126.26, 130.14, 130.38, 130.51, 133.43, 134.03, 136.06, 147.95, 147.99 (Bn), 192.78 (HC=O) ppm. IR (ATR): $\tilde{\nu}_{max}$ = 3406, 2361, 1765, 1714, 1294, 1177, 1152, 1025, 1004, 821, 763, 733 cm^{-1}.

Synthesis of Compound 20: Compound **19** (50.00 mg, 0.15 mmol) was dissolved in THF (10 mL) before a solution of C_{60} (152.00 mg, 0.22 mmol) in toluene (300 mL) was added. After stirring under the exclusion of light for 30 min, sarcosine (18.00 mg, 0.22 mmol) was added, and the reaction mixture was heated at 110 °C under the exclusion of air and light for 22 h. The monoadduct was separated from C_{60} and higher adducts by column chromatography [SiO_2; toluene → toluene/EtOAc (1:1)]. The resulting brown solid was dissolved in CS_2 and precipitated with *n*-pentane to remove solvent residues. Yield: 46 mg (29%). ^{1}H NMR (400 MHz, CS_2/[D_8]THF, 25 °C): δ = 4.77 (d, $^2J_{H,H}$ = 9.5 Hz, 1 H, NCH_2), 2.94 (s, 3 H, CH_3), 4.97 (s, 1 H, NCH), 4.98 (d, $^2J_{H,H}$ = 9.5 Hz, 1 H, NCH_2), 7.12 (d, $^3J_{H,H}$ = 8.6 Hz, 2 H, Bn), 7.46 (d, $^3J_{H,H}$ = 8.8 Hz, 2 H, Bn), 7.54 (d, $^3J_{H,H}$ = 8.55 Hz, 2 H, Bn), 7.77 (d, $^3J_{H,H}$ = 6.7 Hz, 2 H, Bn), 10.51 (s, 2 H, NH) ppm. ^{13}C NMR (100.5 MHz, CS_2/[D_8]THF, 25 °C): δ = 62.01 (CH_3), 69.10, 70.40 (sp^3C C_{60}), 78.16 (NCH), 90.12, 90.57 (C≡C), 123.50, 123.67, 129.08, 129.37, 131.80, 133.72, 135.66, 136.02, 136.47, 136.64 (Bn), 140.07, 140.28, 140.35, 141.34, 141.66, 141.75, 141.97, 142.17, 142.28, 142.69, 142.75, 143.13, 143.26, 144.45, 144.70, 144.73, 144.77, 144.84,

145.23, 145.33, 145.38, 145.51, 145.66, 145.82, 145.99, 146.09, 146.14, 146.25, 146.31, 146.76, 147.00 (sp^2C C_{60}), 147.22, 148.58 (NC=O) ppm. MS (FAB): *m/z* = 1073 $[M]^+$. UV/Vis (CH_2Cl_2): λ = 430.45, 318.51, 314.77, 239.23, 224.52 nm. IR (ATR): $\tilde{\nu}_{max}$ = 2949, 2781, 2361, 2342, 1716, 1645, 1457, 1435, 1276, 1261, 764, 750 cm^{-1}.

Supporting Information (see footnote on the first page of this article): ^{1}H and ^{13}C NMR spectra of porphyrin **13** (Figures S1 and S2), ^{1}H NMR spectrum of porphyrin **16** (Figure S3), Scatchard plots of the systems **10·L$_2$** (**L** = **21**, **22**, and **23**) (Figure S4).

Acknowledgments

We the thank the SFB 583 and the Cluster of Excellence "Engineering of Advanced Materials" for financial support.

[1] J. A. A. W. Elemans, R. Van Hameren, R. J. M. Nolte, A. E. Rowan, *Adv. Mater.* **2006**, *18*, 1251.
[2] J. Koepke, X. Hu, C. Muenke, K. Schulten, H. Michel, *Structure* **1996**, *4*, 581.
[3] M.-S. Choi, T. Yamazaki, I. Yamazaki, T. Aida, *Angew. Chem.* **2004**, *116*, 152.
[4] A. Satake, Y. Kobuke, *Tetrahedron* **2005**, *61*, 13.
[5] a) P. J. Dandliker, F. Diederich, M. Gross, C. B. Knobler, A. Louati, E. M. Sanford, *Angew. Chem.* **1994**, *106*, 1821; *Angew. Chem. Int. Ed. Engl.* **1994**, *33*, 1739–1742; b) P. J. Dandliker, F. Diederich, M. Gross, J. P. Gisselbrecht, A. Louati, *Angew. Chem.* **1995**, *107*, 2906–2909; *Angew. Chem. Int. Ed. Engl.* **1995**, *34*, 2725; c) A. Zingg, B. Felber, L. Fu, J. P. Collman, F. Diederich, *Helv. Chim. Acta* **2002**, *85*, 333; d) P. Weyermann, F. Diederich, *Helv. Chim. Acta* **2002**, *85*, 599.
[6] a) G. J. Hawker, J. M. J. Fréchet, *J. Am. Chem. Soc.* **1990**, *112*, 7638; b) K. W. Pollak, J. W. Leon, J. M. J. Fréchet, M. Maskus, H. D. Abruña, *Chem. Mater.* **1998**, *10*, 30; c) R. H. Jin, T. Aida, S. Inoue, *J. Chem. Soc., Chem. Commun.* **1993**, 1260–1264; d) Y. Tomoyose, D. L. Jiang, R. H. Jin, T. Aida, T. Yamashita, K. Horie, E. Yashima, Y. Okamoto, *Macromolecules* **1996**, *29*, 5236.
[7] F. Li, S. I. Yang, Y. Ciringh, J. Seth, C. H. Martin III, D. L. Singh, D. Kim, R. R. Birge, D. F. Bocian, D. Holten, J. S. Lindsey, *J. Am. Chem. Soc.* **1998**, *120*, 10001.
[8] G. Slobodkin, F. Erkan, A. D. Hamilton, *New J. Chem.* **1992**, *16*, 643.
[9] P. Tecilla, R. P. Dixon, G. Slobodkin, D. S. Alavi, D. H. Waldeck, A. D. Hamilton, *J. Am. Chem. Soc.* **1990**, *112*, 9408.
[10] a) K. Hager, A. Franz, A. Hirsch, *Chem. Eur. J.* **2006**, *12*, 2663; b) K. Maurer, K. Hager, A. Hirsch, *Eur. J. Org. Chem.* **2006**, *15*, 3338.
[11] a) D. Dolphin, *The Porphyrins*, Academic Press, **1978**; b) K. M. Kadish, K. M. Smith, R. Guillard (Eds.), *The Porphyrin Handbook*, Academic Press, San Diego, **2000**.
[12] a) P. M. Allemand, A. Koch, F. Wudl, Y. Rubin, F. Diederich, M. M. Alvarez, S. J. Anz, R. L. Whetten, *J. Am. Chem. Soc.* **1991**, *113*, 1050; b) Q. Xie, E. Perez Cordero, L. Echegoyen, *J. Am. Chem. Soc.* **1992**, *114*, 3978.
[13] a) H. Imahori, K. Hagiwara, T. Akiyama, S. Taniguchi, S. Okada, M. Shirakawa, Y. Sakata, *Chem. Phys. Lett.* **1996**, *263*, 545; b) D. M. Guldi, K. D. Asmus, *J. Am. Chem. Soc.* **1997**, *119*, 5744; c) H. Imahori, M. E. El-Khouly, M. Fujitsuka, O. Ito, Y. Sakata, S. Fukuzumi, *J. Phys. Chem. A* **2001**, *105*, 325.
[14] a) H. Imahori, D. M. Guldi, K. Tamaki, Y. Yoshida, C. Luo, Y. Sakata, S. Fukuzumi, *J. Am. Chem. Soc.* **2001**, *123*, 2571; b) T. D. M. Bell, T. A. Smith, K. P. Ghiggino, M. G. Ranasinghe, M. J. Shephard, M. N. Paddon Row, *Chem. Phys. Lett.* **1997**, *268*, 223; c) P. S. Baran, R. R. Monaco, A. U. Khan, D. I. Schuster, S. R. Wilson, *J. Am. Chem. Soc.* **1997**, *119*, 8363; d) S. Higashida, H. Imahori, T. Kandea, Y. Sakata, *Chem. Lett.* **1998**, 605; e) K. Tamaki, H. Imahori, Y. Nishimura, I. Yamazaki, A. Shimomura, T. Okada, Y. Sakata, *Chem. Lett.* **1999**, 227; f) R. Fong, D. I. Schuster, S. R. Wilson, *Org. Lett.* **1999**, *1*, 729; g) M. Wedel, F. P. Montforts, *Tetrahedron Lett.* **1999**, *40*, 7071; h) N. Armaroli, G. Marconi, L. Echegoyen, J.-P. Bourgeois, F. Diederich, *Chem. Eur. J.* **2000**, *6*, 1629.
[15] a) A. P. H. Schenning, J. v. Herrikhuyzen, P. Jonkheim, Z. Chen, F. Würthner, E. W. Meijer, *J. Am. Chem. Soc.* **2002**, *124*, 10252; b) D. M. Guldi, N. Martín, *J. Mater. Chem.* **2002**, *12*, 1978; c) J. L. Sessler, M. Sathiosatam, C. T. Brown, T. A. Rhodes, G. Wiederrecht, *J. Am. Chem. Soc.* **2002**, *124*, 3655; d) A. J. Myles, N. R. Branda, *J. Am. Chem. Soc.* **2001**, *123*, 177; e) T. H. Ghaddar, E. W. Castner, S. S. Isied, *J. Am. Chem. Soc.* **2000**, *122*, 1233; f) J. L. Sessler, J. Jayawickramarajah, A. Gouloumis, T. Torres, D. M. Guldi, S. Maldonado, K. J. Stevenson, *Chem. Commun.* **2005**, 1892.
[16] K. Hager, U. Hartnagel, A. Hirsch, *Eur. J. Org. Chem.* **2007**, 1942.
[17] a) F. Wessendorf, J.-F. Gnichwitz, G. H. Sarova, K. Hager, U. Hartnagel, D. M. Guldi, A. Hirsch, *J. Am. Chem. Soc.* **2007**, *129*, 16057; b) J.-F. Gnichwitz, M. Wiepolski, K. Hartnagel, U. Hartnagel, D. M. Guldi, A. Hirsch, *J. Am. Chem. Soc.* **2008**, *130*, 8491.
[18] F. D'Souza, R. Chitta, S. Gadde, A. L. Mc Carthy, P. A. Karr, M. E. Zandler, A. S. D. Sandanayaka, Y. Araki, O. Ito, *J. Phys. Chem. B* **2006**, *110*, 5905.
[19] F. Wessendorf, A. Hirsch, *Tetrahedron* **2008**, *64*, 11480.
[20] A. Kraft, *Liebigs Ann./Recueil* **1997**, 1463.
[21] A. Dirksen, U. Hahn, F. Schwanke, M. Nieger, J. N. H. Reek, F. Vögtle, L. de Cola, *Chem. Eur. J.* **2004**, *10*, 2036.
[22] J. S. Lindsey, I. C. Schreimann, H. C. Hsu, P. C. Kearney, A. M. Marguerettaz, *J. Org. Chem.* **1987**, *52*, 827.
[23] N. Jux, *Org. Lett.* **2000**, *2*, 2129.
[24] a) C. G. Vogel, A. L. Searby, *Inorg. Chem.* **1973**, *12*, 936; b) C. G. Vogel, J. R. Stahlbusch, *Inorg. Chem.* **1977**, *16*, 950.
[25] a) W. R. Scheidt, C. W. Eigenbort, M. Ogiso, K. Hatano, *Bull. Chem. Soc. Jpn.* **1987**, *60*, 3259; b) S. G. DiMagno, V. S.-Y. Lin, M. J. Therien, *J. Am. Chem. Soc.* **1993**, *115*, 2513; c) P. N. Taylor, A. P. Wylie, J. Huuskonen, H. L. Anderson, *Angew. Chem. Int. Ed.* **1998**, *37*, 986.
[26] *Hyperchem Professional 7.5 for Windows*, Hypercube Inc., Copyright **2002**, http://www.hyper.com, **2004**.
[27] *Spartan 06 for Windows and Linux*, Wavefunction Inc., Copyright **2006**.
[28] M. J. Plater, J. P. Sinclair, S. Aiken, T. Gelbrich, M. B. Hursthouse, *Tetrahedron* **2004**, *60*, 6385.
[29] L. Fielding, *Tetrahedron* **2000**, *56*, 6151.
[30] V. Behrl, M. Schmutz, M. J. Krische, R. G. Khoury, J. M. Lehn, *Chem. Eur. J.* **2002**, *8*,1227.
[31] B. Perlmutter-Hayman, *Acc. Chem. Res.* **1986**, *19*,90–96.
[32] J. D. Badjiić, A. Nelson, S. J. Cantrill, W. B. Turnbull, J. F. Stoddart, *Acc. Chem. Res.* **2005**, *38*, 723.
[33] H.-J. Schneider, A. Yatsimirsky, *Principles and Methods in Supramolecular Chemistry*, Wiley, Chichester, **2000**.
[34] V. P. Solov'ev, E. A. Vnuk, N. N. Strakhova, O. A. Reavsky, *VINITI*, Moscow, **1991**.
[35] V. P. Solov'ev, V. E. Baulin, N. N. Strakhova, V. P. Kazachenko, V. K. Belsky, A. A. Varnek, T. A. Volkova, G. Wipff, *J. Chem. Soc. Perkin Trans. 2* **1998**, 1489.
[36] We know that **15**, in contrast to **10**, is not a single species but rather a multicomponent system held together by strong intermolecular interactions, but we assume that the self-assembly processes are comparable to the association processes involving *cis* analogue **10**.
[37] C. A. Hunter, H.-L. Anderson, *Angew. Chem. Int. Ed.* **2009**, *48*, 7488.
[38] G. Scatchard, *Ann. N. Y. Acad. Sci.* **1949**, *51*, 660.
[39] a) A. V. Hill, *Biochem. J.* **1913**, *7*, 471; b) A. V. Hill, *J. Physiol. (London)* **1910**, *40*, 4.

[40] a) V. Chukharev, N. V. Tkachenko, A. Efimov, D. M. Guldi, A. Hirsch, M. Scheloske, H. Lemmetyinen, *J. Phys. Chem. B* **2004**, *108*, 16377; b) H. Imahori, N. V. Tkachenko, V. Vehmanen, K. Tamaki, H. Lemmetyinen, Y. Sakata, S. Fukuzumi, *J. Phys. Chem. A* **2001**, *105*, 1750; c) V. Chukharev, N. V. Tkachenko, A. Efimov, H. Lemmetyinen, *Chem. Phys. Lett.* **2005**, *411*, 501; d) D. M. Guldi, A. Hirsch, M. Scheloske, E. Dietel, A. Troisi, F. Zerbetto, M. Prato, *Chem. Eur. J.* **2003**, *9*, 4968.

[41] K. A. Connors, *Binding Constants*, Wiley, New York, **1987**.

[42] a) C. Atienza, N. Martín, M. Wielopolski, N. Haworth, T. Clark, D. M. Guldi, *Chem. Commun.* **2006**, 3202; b) M. Wielopolski, C. Atienza, T. Clark, D. M. Guldi, N. Martín, *Chem. Eur. J.* **2008**, *14*, 6379.

[43] B. Valeur, *Molecular Fluorescence*, Wiley-VCH, Weinhein, **2002**.

[44] a) D. M. Guldi, H. Hungerbuehler, K.-D. Asmus, *J. Phys. Chem.* **1995**, *99*, 9380; b) D. M. Guldi, M. Prato, *Acc. Chem. Res.* **2000**, *33*, 695; c) S. Fukuzumi, H. Imahori, H. Yamada, M. E. El-Khouly, M. Fujitsuka, O. Ito, D. M. Guldi, *J. Am. Chem. Soc.* **2001**, *123*, 2571.

Received: February 20, 2010
Published Online: July 26, 2010

